Original Paper

Helmut Schöllnberger[1,2], Jan Christian Kaiser[1], Markus Eidemüller[1], Lydia B. Zablotska[3]

Radio-biologically Motivated Modeling of Radiation Risks of Mortality From Ischemic Heart Diseases in the Canadian Fluoroscopy Cohort Study

[1]   Helmholtz Zentrum München, Department of Radiation Sciences, Institute of Radiation Medicine, Ingolstädter Landstrasse 1, D-85764 Neuherberg, Germany

[2]   Federal Office for Radiation Protection, Division UR - Environmental Radioactivity, Ingolstädter Landstrasse 1, D-85764 Neuherberg, Germany

[3]   University of California, Department of Epidemiology and Biostatistics, School of Medicine, San Francisco, 550 16th Street, CA 94143, United States of America

H. Schöllnberger (✉)
Helmholtz Zentrum München, Department of Radiation Sciences, Institute of Radiation Medicine, Ingolstädter Landstrasse 1, D-85764 Neuherberg, Germany
Tel: +49 (0)89-3187-2765
hschoellnberger@bfs.de;
schoellnberger@helmholtz-muenchen.de

ORCID 0000-0002-4398-6565 (H. Schöllnberger)
ORCID 0000-0003-0359-2251 (J.C. Kaiser)
ORCID 0000-0003-0249-3710 (M. Eidemüller)
ORCID 0000-0002-0778-1108 (L.B. Zablotska)

Abstract

Recent analyses of the Canadian Fluoroscopy Cohort Study reported significantly increased radiation risks of mortality from ischemic heart diseases (IHD) with a linear dose-response adjusted for dose-fractionation. This cohort includes 63,707 tuberculosis patients from Canada who were exposed to low-to-moderate-dose fractionated x-rays in 1930s-1950s and were followed-up for death from non-cancer causes during 1950–1987. In the current analysis, we scrutinized the assumption of linearity by analyzing a series of radio-biologically motivated nonlinear dose-response models to get a better understanding of the impact of radiation damage on IHD. The models were weighted according to their quality of fit and were then mathematically superposed applying the multi-model inference (MMI) technique. Our results indicated an essentially linear dose-response relationship for IHD mortality at low and medium doses and a supra-linear relationship at higher doses (>1.5 Gy). At 5 Gy, the estimated radiation risks were 5-fold higher compared to the linear no-threshold (LNT) model. This is the largest study of patients exposed to fractionated low-to-moderate doses of radiation. Our analyses confirm previously reported significantly increased radiation risks of IHD from doses similar to those from diagnostic radiation procedures.

Keywords Ionizing radiation, Ischemic heart diseases, LNT model, Multi-model inference, Nonlinear dose-response

Introduction

One of the most important questions in radiation research relates to the shape of the dose-response for different detrimental health outcomes at low exposures levels. Various international radiation protection organizations use the linear no-threshold (LNT) model to predict risks of cancer after ionizing radiation (IR) exposures (NCRP 2018, Shore et al. 2018, 2019, ICRP 2005, UNSCEAR 2000). However, the most recent analysis of the Life Span Study (LSS) data suggests a significant quadratic upward curvature, especially for the incidence of all solid cancers in males (Grant et al. 2017). For cardiovascular diseases (CVD), doses above 5 Gy IR have been shown to be associated with a significantly elevated risk (HPA 2010). At doses between 0.5 and 5 Gy, there is clear evidence for an increased risk (HPA 2010, Kreuzer et al. 2015, Azizova et al. 2015a, 2015b, Moseeva et al. 2014). Radiation risks at low (<0.1 Gy) and low-to-moderate (0.1-0.5 Gy) doses have been examined only in a few studies with considerable discrepancies in findings and require further research (for example, Shimizu et al. 2010, Mitchel et al. 2011, 2013, Little et al. 2012, Ozasa et al. 2012, 2017, Schöllnberger et al. 2012, Schöllnberger et al. 2018, Simonetto et al. 2014, 2015, Takahashi et al. 2017, Gillies et al. 2017). In this context, the question whether even smallest doses of IR may increase the risk of CVD or whether nonlinear dose-response curves may be better suited to describe the health risk is of special interest. There could also be a threshold for the dose below which radiation may have no effect, or lead to either a strongly elevated risk or a protective effect. Such questions are of great importance for radiation protection, especially against the rising worldwide use of IR in medical applications. They are also relevant for occupationally exposed groups of individuals. For CVD, the question of the shape of the dose-response is as important as it is for cancer because even though relative radiation risks of CVD are smaller than radiation risks of cancer (Ozasa et al. 2012), the overall burden of disease is much larger due to high background rates of CVD in Western populations (World Health Organization 2013).

Recently significantly elevated risks of death from ischemic heart diseases (IHD) in a cohort of tuberculosis patients from Canada exposed to low-to-moderate doses of highly-fractionated x-ray radiation from repeated chest fluoroscopies were reported (Zablotska et al. 2014). The reported dose-response was strictly linear, and researchers described a novel finding of a significant inverse dose-fractionation association in IHD mortality (Zablotska et al. 2014). The aim of the present study is to investigate radiation-associated risk of IHD in the Canadian Fluoroscopy Cohort Study (CFCS) with a larger set of radio-biologically motivated dose-response models and to comprehensively characterize model uncertainties using multi-model inference (MMI, Burnham and Anderson 2002, Claeskens and Hjort 2008, Walsh and Kaiser 2011).

Materials and methods

Data sources

The CFCS data have been described in detail elsewhere (Zablotska et al. 2014). The cohort includes 63,707 tuberculosis patients from Canada who were first treated for tuberculosis between 1930 and 1952 and could have received multiple fluoroscopic x-ray examinations to maintain therapeutic pneumothorax, one of the preferred treatments in the pre-antibiotic era. Most individuals in the cohort were born between 1920 and 1929 (see Table 2 in Zablotska et al. 2014). Absorbed lung doses from fluoroscopic examinations were estimated for each patient for each year since first admission for treatment of tuberculosis (Zablotska et al. 2014). For each lung dose to be estimated 100,000 simulations were carried out and an arithmetic mean of all simulations was used for dose-response analyses. The lung dose was

3

used because it should be a reasonable surrogate for doses to the heart and associated major blood vessels (Zablotska et al. 2014). There could be substantial uncertainties in dose estimates. These are partially accounted for in the dose-estimation methods, where doses were estimated using Monte Carlo simulation techniques, which sampled from probability distributions of various data sources and should provide a reasonable estimate of radiation doses to the lung and heart. As stated by Zablotska et al. (2014), the impact of errors in exposure estimates in dosimetry was estimated in previous studies and shown to be relatively small and primarily of Berkson type (Howe and McLaughlin 1996) and therefore unlikely to introduce a substantial bias in risk estimates (Carroll et al. 2006).

Thirty-nine percent of the cohort (24,932 patients) were exposed to at least one fluoroscopy while the remaining 38,775 are considered unexposed to radiation from fluoroscopy. On average, exposed patients were treated 64 times with a typical fluoroscopic examination delivering a mean lung dose of 0.0125 Gy at a dose rate of approximately 0.6 mGy second^{-1}. The mean cumulative person-year-weighted lagged lung dose among exposed was 0.79 Gy (range, 0 – 11.6 Gy). Doses were lagged by 10 years, a minimal latent period that has been used in several studies of long-term risks of radiation exposure on cancer and noncancer mortality risk (Zablotska et al. 2014, Little et al. 2012, Darby et al. 2010).

Study participants had to be alive at the start of follow-up in 1950 and were followed up for mortality until the end of 1987 with 1,902,251.68 person-years. During this time, 5818 deaths from IHD (ICD-9 codes 410–414 und 429.2) were identified through a linkage with the Canadian Mortality Database. The cohort was evenly split between men and women. Patient age at first admission for tuberculosis treatment ranged from 1 to 81 years. Additional characteristics of the CFCS are provided in Table S1 of the Online Resource.

Statistical methods

The present analysis applied the same dataset cross-classified by sex, Canadian province of most admissions (Nova Scotia, other), type of tuberculosis diagnosis (pulmonary, nonpulmonary), stage of tuberculosis (minimal, moderate, advanced, or not specified), smoking status (unknown, non-smoker, smoker), age at first exposure (0–4, 5–9, 10–19, or 20–87 years), attained age (0–24, 25–29, … 80–84, or 85–100 years), calendar year at risk (1950–1954, 1955–1959, . . . 1980–1984, or 1985–1987), duration of fluoroscopy screenings, and 10-year cumulative lagged lung dose as (Zablotska et al. 2014). Poisson regression was based on time-dependent person-year–weighted mean cumulative dose in cross-classified cells, using excess relative risk (ERR) models in combination with a parametric baseline model[1]. The general form of an ERR model is $h = h_0 \times (1 + ERR(D, Z))$, where h is the total

---

[1] In this study, mortality follow-up was conducted through record linkage with the Canadian Mortality Database using probabilistic linkage. The term "record linkage" refers to the process of comparing two or more records which contain identifying information to determine whether those records refer to the same individual enrolled in a cohort study. In the absence of personal identifying numbers which would allow definitive linkage to mortality outcomes (social insurance numbers were not introduced in Canada until 1964 while the study is based on the medical records for patients first admitted for treatment during 1930-1952), study investigators used a combination of identifying items such as surname; given name; day, month, and year of birth to conduct a linkage. Each pair of linked records was assigned a probabilistic weight which depends on the likelihood of the link being true (Howe 1998). A cutoff value was then used to separate possibly true links with higher linkage weights from those less likely to be true. A higher cutoff point for the internal dose-response analysis was used to avoid dilution of any association due to the presence of false positives

hazard function, h_0 is the parametric baseline model. $ERR(D, Z)$ describes the change of the hazard function with cumulative lagged lung dose D allowing for dose-effect modification by co-factor(s) Z, such as sex, age at first exposure or dose-fractionation so that $ERR(D, Z) = err(D) \times \varepsilon(Z)$. Here, $err(D)$ represents the dose-response and $\varepsilon(Z)$ contains the dose-effect modifiers[2] (DEMs). A parametric baseline model had been developed to analyze the risk for IHD in the Mayak Workers Cohort (Simonetto et al. 2014). It was taken as guidance for developing a parametric baseline model for the CFCS data. Both models for cohorts Mayak and CFCS are provided on pages 4-6 of the Online Resource. The baseline model in equation (S4) of the Online Resource was combined with the LNT model and adjusted for dose-fractionation (Zablotska et al. 2014):

$$h = h_0\{1 + \beta_1 \times D \times \exp[\beta_2(drate - 0.2)]\} \tag{1}$$

Here, β_1 denotes the slope of the linear dose-response and β_2 is the parameter associated with the DEM $drate - 0.2$. Parameter $drate$ represents the dose-fractionation, a surrogate for dose rate, defined as $drate := D\ time^{-1}$ where $time$ is the overall duration of fluoroscopic procedures[3]. The unit of $drate$ is Gy yr^{-1}. By centering $drate$ parameter β_1 corresponds to the risk for a patient with radiation exposures at 0.2 Gy yr^{-1}, i.e. approximately 16 fluoroscopic procedures per year (Zablotska et al. 2014).

Subsequently, the dose-response model from equation (1) (i.e. $\beta_1 \times D$) was substituted by the models in Figure 1 (Q-model – Gompertz model). They were chosen with care to reflect as many biologically plausible shapes for dose-responses as possible, including supralinear and sublinear models. Motivations for these models from the biological scientific literature are provided in Table 1 and in the *Discussion* section. The mathematical forms and names of the functions illustrated in Figure 1 are given in column 1 and 2 of Table 1, respectively. Columns 3 and 4 of Table 1 state which types of radiation biological experiments have previously provided evidence for applying these functions in the present analysis, and the relevant citations of the biology papers, respectively. Mathematical details of all models in Figure 1 are also given on page 7 of the Online Resource; that also includes the categorical model. The threshold-dose parameter (D_{th}) contained in some models (LTH, smooth step, sigmoid, hormesis, two-line spline) was optimized during the model fits. The smooth step model was implemented as a modified hyperbolic tangent function, which can accommodate various different shapes. With this function, a step is not imposed *a priori* but results from fitting that model to data.

Multi-model inference (MMI) method

(i.e., false linkages); the change in cutoff would not be expected to bias estimates of relative risk. Under quite general conditions, potentially substantial bias could be introduced by using absolute risk models. Therefore, analyses with EAR models should not be performed with the CFCS data because the linkage of the cohort with the mortality registry is probabilistic which could affect absolute mortality but not relative mortality models (Zablotska et al. 2014).

[2] Co-factor(s) Z, such as sex, age at first exposure or dose-fractionation are often referred to in radiation epidemiology as *risk effect modifiers* because they are factors that modulate the main central risk per unit dose estimate.

[3] Duration of fluoroscopic procedures respectively fluoroscopy screenings refers to the timespan over which fluoroscopic examinations were provided.

The term MMI was coined to describe a frequentist approach to model averaging (Burnham and Anderson 2002), and has been applied to model selection in radiobiology. In contrast to Bayesian model averaging (BMA) (Hoeting et al 1999), which is based on the evaluation of model-specific marginal likelihood functions to determine a model average, MMI relies on the Akaike Information Criterion (AIC; Akaike 1973, 1974) and AIC-based model weights for model building. BMA is computationally more demanding and only a few radiation epidemiological studies have used it to account for uncertainties in dose estimation (Little et al. 2014, 2015, Land et al. 2015, Hoffmann et al. 2017). Both BMA and MMI apply the concept of Occam's group (Madigan and Raftery 1994, Hoeting et al 1999, Noble et al. 2009, Kaiser and Walsh 2013), where a group of models deemed adequate for averaging is selected from a larger group of candidate models (see Figure 1). The methods of picking models for Occam's group can vary. For example, Walsh and Kaiser (2011) selected all published models, which have been applied to the same LSS dataset for the same endpoint, whereas Kaiser and Walsh (2013) developed a rigorous selection process based on likelihood ratio tests (LRTs).

The shape of the MMI-derived dose-response is more reliably determined than the shape for any individual dose-response because the MMI dose-response shape accounts for strengths of evidence for each of the contributing dose-response shapes. MMI also provides a more comprehensive characterization of model uncertainties by accounting for possible bias from model selection. It is a statistical method of superposing different models that all describe a certain data set about equally well (Burnham and Anderson 2002, Claeskens and Hjort 2008). In the present study the MMI approach aims to detect nonlinearities in the dose-response by combining biologically-plausible dose-responses based on goodness-of-fit.

Model selection

To assess the influence of model selection criteria on the risk estimates, we used two approaches. In the *sparse model approach,* candidate dose-response models from Figure 1 were compared using the LRT at a 95% confidence level. With this method, a small set of final non-nested models with highly significant dose-responses was identified for Occam's group. Specifically, for each final non-nested model we calculated the AIC using the formula:
$AIC = dev + 2 \times N_{par}$,
where dev is the final deviance and N_{par} is the number of model parameters. Models with smaller AIC are favored based on fit (via dev) and parameter parsimony (models with more parameters get punished by the factor $2 \times N_{par}$) (Walsh 2007). For a set of final non-nested models, AIC-weights are calculated; models with smaller AIC are assigned a larger weight (see page 8 of the Online Resource). The resulting weights, multiplied by a factor of 10^4, gave a number of samples for risk estimates to be generated by uncertainty distribution simulations. We then combined model-specific probability density functions into one dataset. The resulting probability density distribution represents all uncertainties arising from the different models and their superposition. Central risk estimates from MMI were calculated from AIC-weighted maximum likelihood estimates (MLE) for single risk models. 95% confidence intervals (CI) were derived from the final merged MMI probability density distributions.

In the second, *rich model approach*, an LRT-based reduction of dose-response parameters of the candidate models was not performed. The AIC was calculated for each different model fit together with the AIC-weights. Models with bilateral AIC-weights smaller than 5% did not survive the selection process; all others were included into the set of final non-nested models. This approach leads to a larger number of models deemed suitable for MMI. The calculation of AIC-weights for the two sets (or Occam's groups) of dose-response

models based on both approaches ("sparse" versus "rich") is detailed on page 8 of the Online Resource. The software used to perform all analyses is briefly introduced on page 9 of the Online Resource.

Results

Similarly to the previously published results (Zablotska et al. 2014), the slope parameter β_1 was not significant without adjustment for dose-fractionation (β_1 = –0.046 Gy^{-1}, Table 2). Adjustment led to a significant *ERR* per dose = 0.182 Gy^{-1} with 95% CI: 0.049, 0.325 (Table 2) (*ERR* per dose = 0.176 Gy^{-1} in Zablotska et al. 2014). Subsequently, the LNT model from equation (1) was substituted by all other models from Figure 1, keeping the DEM *drate* – 0.2.

Considering the relations in Figure S1 of the Online Resource and a sparse model approach, four final non-nested models survived the selection process and were included into Occam's group: LNT, Q, two-line spline[4] and the Gompertz models. For these four models, the model parameters (baseline and radiation-associated), their MLE and symmetric, Wald-type standard errors are provided in Table S2 of the Online Resource. Details related to model selection according to the sparse model approach are provided in the Online Resource (see pages 8, 14 and 15 and Table S3).

According to the rich model approach, 10 models survived the selection process and contributed to MMI with normalized weights provided in Table 3. Figure 2 shows the *ERR* plotted against the cumulative lagged lung dose for the four final non-nested models and for the simulated dose-response curve from MMI, calculated with the sparse and the rich model approaches. Figures 3 and 4 show the best models and MMI for doses <2 and 0.1 Gy, respectively. Table 4 provides risk predictions based on MMI (sparse) and the LNT, Q, two-line spline and Gompertz models. The radiation-associated excess cases according to the four final non-nested models and MMI (sparse) are presented in Table 5.

The Gompertz model had the best fit to the data (Table 3). Both Q and Gompertz models predicted no increase in risk below 0.05 Gy (Figure 4). While both models predicted a sublinear dose-response at low and medium doses up to ~1 Gy, the two-line spline model predicted a risk higher than all other models (Figures 2 and 3). The *ERR* predictions from MMI and LNT model at 0.1 Gy and 1 Gy are identical within their 95% CI (Table 4) and the dose-response from MMI is roughly linear at low doses (Figure 4). At low and medium doses up to ~1 Gy, MMI and the LNT model predict similar risk values (Figure 3). Consequently, up to 1 Gy both models (LNT and MMI) predict very similar excess cases (Table 5). At doses >1.5 Gy, the dose-response from MMI predicted a higher risk compared to the LNT model (Figures 2 and 3, Table 4). For the entire dose range, the dose-responses from the MMI calculated using both the sparse and the rich model approaches were similar to each other (Figures 2 to 4). For example, at 1 Gy, MMI predicted an *ERR* of 0.216 with 95% CI: 0.062, 0.48 and *ERR* = 0.218 with 95% CI: 0.058, 0.473, for rich and sparse model approaches, respectively.

Figure S2 of the Online Resource shows the baseline cases as predicted by the ERR-LNT model versus attained age with the secular trend together with crude rates.

---

[4] It is noted that the two-line spline model is nested with the LNT model. This can be seen in Figure S1 of the Online Resource: The two-line spline model is nested with the LTH model and the latter is nested with the LNT model (in general, Model A is nested in Model B if the parameters in Model A are a subset of the parameters in Model B). The reason why the two-line spline model was nonetheless included into Occam's group is explained on pages 15 and 16 of the Online Resource.

Discussion

CFCS is the largest cohort of patients exposed to fractionated low-to-moderate doses of IR via fluoroscopic x-rays. About 15.5% of exposed CFCS patients were exposed to doses <0.1 Gy and thus provide direct evidence of possible risks from low-dose exposures such as CT scans (like fluoroscopic examinations, CT scans in their most commonly known form apply x-rays). We examined 10 biologically-plausible dose-response models together with a categorical model. At low and medium doses the MMI technique predicted an almost linear dose-response.

While the sparse model selection approach led to a set of four final non-nested models, the rich model approach yielded an Occam's group that contained ten out of the eleven dose-response models that were fitted to the data. Both sets of dose-response models describe the data approximately equally well (see values of ΔAIC in Table 3).

The reason for MMI-predicted risks being significantly higher compared to the LNT model at doses >1.5 Gy is the relatively strong contributions of the Q, two-line spline and Gompertz models to the MMI (88% of the total, Table 3). At 5 Gy, MMI predicted an approximately 5-fold risk compared to the LNT model, at 10 Gy a 6-fold risk.

To better understand predicted radiation risks at higher doses, we used a restriction analysis based on cohort data with restricted dose-ranges and observed that the second slope of the two-line spline model (β_2) was driven by high doses (>2 Gy). When restricting the data to doses smaller than 2 Gy, the first slope (β_1) of this model became very similar to the slope of the LNT model (results not shown). The LNT model was influenced mostly by doses <2 Gy. The higher doses hardly influence the slope of the LNT model due to the lower number of cases in this dose range (212 cases out of 5818). Thus, the fit of the two-line spline model, which predicts a more than two times higher number of excess cases than the LNT model (Table 5), is consistent with the fit of the latter model.

The present study applied a larger range of biologically-realistic smooth dose-response models (Figure 1). Exploring a larger range of different dose-response models is motivated by the following biological findings, which are summarized in Table 1. The use of the LNT model finds support from the study of Stewart et al. (2006). These researchers investigated the effects of a high dose (14 Gy) exposure on the development of atherosclerotic plaques (number of lesions, plaque area and plaque composition) in ApoE$^{-/-}$ mice. They found that after the high dose exposure the mean number of atherosclerotic lesions (initial plus advanced) in carotid arteries of irradiated mice was significantly larger than in age- and sex-matched controls. Their study also revealed a significantly enhanced inflammatory content and plaque hemorrhage of irradiated carotid artery lesions compared to controls (Stewart et al. 2006). Because only one high dose exposure was investigated these findings infer an LNT-like dose-response. Analyses with a quadratic or linear-quadratic model are supported by the work of Hoving et al. (2008). The found that the number of initial atherosclerotic lesions and the plaque area in female mice 30 weeks after exposure to 0, 8 or 14 Gy clearly exhibit a dose-response consistent with a quadratic or linear-quadratic response (see panels B and E in their Figure 3). In addition, some of the findings reported by Hoving et al. (2008) support the use of an LNT model. The specific feature of the linear-quadratic model that it can exhibit a U-shape at low doses is supported by the findings of Mitchel et al. (2011, 2013) and Ebrahimian et al. (2018). The findings of these three studies will be briefly described below in the context of the hormesis model. The application of the linear-exponential model is justified because of the findings by Mancuso et al. (2015) related to atherogenesis in ApoE$^{-/-}$ mice. Although the pattern of radiation-induced aortic alterations and their severity increased at 6 Gy compared with a 20-fold lower dose of 0.3 Gy, their results tend to be far from linearity and suggest that lower doses may be more damaging than

8

predicted by a linear dose response (Mancuso et al. 2015). The LTH model is another realistic possibility for a dose-response related to radio-epidemiological cohorts given the findings from animal studies on protective anti-inflammatory effects induced by low doses of radiation (Mitchel et al. 2011, 2013, Mathias et al. 2015, Le Gallic et al. 2015, Ebrahimian et al. 2018). Investigating the expression of various inflammatory and thrombotic markers in the heart of ApoE$^{-/-}$ mice, Mathias et al. (2015) provided evidence for anti-inflammatory effects after 0.025 - 0.5 Gy exposures: they found slight decreases of ICAM-1 levels and reduction of Thy 1 expression at these doses. In contrast, an enhancement of MCP-1, TNFα and fibrinogen at 0.05 - 2 Gy indicated a proinflammatory and prothrombotic systemic response (Mathias et al. 2015). In such a situation, a LTH model may describe the data better than the LNT model. Interestingly, Mitchel et al. (2007) reported that their dermatitis data from C57BL/6J mice indicate that low doses may generally produce either no effect or protective effects with respect to this autoimmune-type and age-related non-cancer disease that has been linked to inflammation (Williams et al. 2012). The findings of anti-inflammatory protective effects at low doses (Mitchel et al. 2007, 2011, 2013, Mathias et al. 2015, Le Gallic et al. 2015, Ebrahimian et al. 2018) and detrimental effects at moderate (0.3 Gy) and higher doses (6 Gy) (Mancuso et al. 2015) provide a biological context for applying the smooth step model (Figure 1). A step-type response (with a steep slope) may reflect the distinct dose at which protective mechanisms are lost. Different tissues and different individuals can be expected to have different threshold-doses, leading to an overall smooth transition. While at low doses it is feasible that risk increase may be balanced by a protective decrease as in the LTH model, a smooth transition zone may exist where risk increases steadily, followed by a plateau. The sigmoid model can exhibit similar shapes as the smooth step model. Therefore, the same references are relevant as for the smooth step model (Mitchel et al. 2007, 2011, 2013, Mathias et al. 2015, Le Gallic et al. 2015, Mancuso et al. 2015, Ebrahimian et al. 2018). The empirical hormesis model applied in the current study has been introduced to describe stimulation of plant growth after low-dose herbicide exposures (Brain and Cousens 1989). Dose-responses which allow for protective effects at low doses, such as LQ, hormesis and two-line spline models, can be justified from mouse studies (Mitchel et al. 2011, 2013). Mitchel et al. (2011) exposed ApoE$^{-/-}$ mice to 0.025, 0.05, 0.10 or 0.50 Gy ^{60}Co γ-irradiation at either low dose rate (1.0 mGy min^{-1}) or high dose rate (approximately 0.15 Gy min^{-1}) and investigated biological endpoints associated with atherosclerosis (aortic lesion frequency, size and severity, total serum cholesterol levels and the uptake of lesion lipids by lesion-associated macrophages). In general, low doses given at low dose rate during either early- or late-stage disease were protective, slowing the progression of the disease by one or more of these measures (Mitchel et al. 2011). The influence of low doses (0.025, 0.05, 0.10 or 0.50 Gy) of ^{60}Co γ-irradiation at low dose rate (1.0 mGy min^{-1}) or high dose rate (approximately 0.15 Gy min^{-1}) on atherosclerosis in ApoE$^{-/-}$ mice with reduced *p53* function was investigated by Mitchel et al. (2013). Radiation exposure to doses as low as 25 mGy at early stage disease, at either the high or the low dose rate, inhibited lesion growth, decreased lesion frequency and slowed the progression of lesion severity in the aortic root. In contrast, exposure at late stage disease produced generally detrimental effects. Both low-and high-dose-rate exposures accelerated lesion growth and high dose rate exposures also increased serum cholesterol levels. All effects were highly nonlinear with dose (Mitchel et al. 2013). An increase in anti-inflammatory and anti-oxidative parameters resulting in atherosclerotic plaque size reduction in ApoE$^{-/-}$ mice after chronic exposure to external low-dose γ-radiation was reported by Ebrahimian et al. (2018). Their results suggest that chronic low-dose gamma irradiation induces an upregulation of organism defenses leading to a decrease in inflammation and plaque size. Low-dose induced anti-inflammatory effects which play an

important role in that context are currently intensely studied (see for example the reviews by Rödel et al. 2012a, 2012b, Frey et al. 2015) and have also been reported by Le Gallic et al. (2015) and Mathias et al. (2015). Earlier, low doses of γ-radiation delivered at low dose rates exhibited a protective effect related to chronic ulcerative dermatitis, an inflammatory skin reaction, in C57BL/6 mice, decreasing both disease frequency and severity and extending the lifespan of older animals (Mitchel et al. 2007). The two-line spline model can describe supralinear or sublinear dose-responses (Figure 1) but also linear dependences. Therefore, its application in the present study finds support from the same studies referenced in the context of the LNT model, the linear-exponential, LTH and hormesis models (refer to Table 1). The Gompertz model can exhibit linear, sublinear and smooth step dose-responses but also supralinear responses. Therefore, its use in the present study is motivated by the same biological findings referenced in the context of the LNT model, the linear-quadratic, LTH, smooth step and linear-exponential models, see Table 1.

Interpretation of our findings is limited by the absence of information on important independent risk factors for CVD in the CFCS data (Zablotska et al. 2014), particularly socioeconomic status and smoking. Only a limited amount of information is available on smoking for approximately 20% of the cohort (smoking was therefore not included in the baseline model, in accordance with Zablotska et al. 2014). Some studies suggest that these factors account for a substantial proportion of observed increase in CVD (see for example Yusuf et al. 2004). However, smoking was not associated with radiation (Zablotska et al. 2014), so could not be considered as a confounding variable in the current analyses. Furthermore, numerous recent studies found weak evidence for interaction between radiation and smoking (for example, Kreuzer et al. 2018). The CFCS data also lack information on other important CVD risk factors, such as family history of heart disease, diabetes, high blood pressure, obesity, and cholesterol plasma levels. However, because these factors are unlikely to be associated with radiation dose, they are unlikely to have biased the observed association between exposure and IHD mortality (Zablotska et al. 2014).

Another limitation is that all study participants had tuberculosis. We are aware that the precise relationship of radiation dose to IHD risk in immunocompromised, chronically ill tuberculosis patients may well differ from that in healthy individuals.

Our study findings are also limited by the end of follow-up in 1987 (Zablotska et al. 2014). It is noted that out of the 63,707 tuberculosis patients 34,717 individuals were still alive at the end of follow-up. CFCS study investigators are in the process of extending mortality follow-up by 30 years (1988-2017). In addition, they will also conduct, for the first time, cancer incidence follow-up of the cohort during 1969-2017. New doses to all organs within and outside the field of fluoroscopic irradiation will be estimated using computerized phantoms specific to the CFCS population.

Within the approach of the present study, the dose-fractionation proportionally affects the magnitude of the dose-response function but not the shape of the dose-response. Given evidence of a significant inverse dose-fractionation association in the primary analysis (Zablotska et al. 2014), it seems to be a hypothesis of interest that the dose-response shape might differ by the dose rate, i.e. dose-fractionation (while the person-year-weighted mean dose-fractionation within the whole cohort is 0.109 Gy yr^{-1}, for mean cumulative person-year-weighted lagged lung doses ≤ 0.1 Gy and > 0.1 Gy that quantity is 0.008 Gy yr^{-1} and 0.101 Gy yr^{-1}, respectively). To investigate whether there may be any difference in the shape of the dose-responses at low and high dose-fractionations the analyses of the present study could in principle be repeated within several strata of dose-rate. Zablotska et al. (2014) performed such an analysis and calculated the *ERR* for three categories of dose-fractionation. For IHD an inverse dose-fractionation association was found using the LNT dose-response

model (Table 6 in Zablotska et al. 2014). While such an effort is beyond the scope of the present study, there is also concern that such an in-depth analysis performed in the context of MMI may outstrip the CFCS data in terms of their ability to characterize risk of subsequent IHD in meaningful populations due to the above mentioned absence of information on classical modifiable cardiovascular risk factors such as lipids, hypertension, diabetes, abdominal obesity, diet, psychosocial factors, etc. as well as family history of IHD.

Generally, inference based on a set of multiple plausible models is a sound alternative to inference relying only on a single "best" model when the uncertainty in the model selection is large. The pitfall of using the MMI approach is, however, related to that specific aspect: The subjectivity of the model selection. In the present study, this problem is addressed with a two-tiered strategy. On the one hand, as already stated above, the models in Figure 1 were carefully chosen to reflect as many biologically plausible shapes for dose-responses as possible. On the other hand MMI was applied in two different approaches, sparse and rich, as described in the *Materials and methods* section. In the center of the case-weighted means (case-weighted mean age, case-weighted mean dose, etc.) all models yield similar risks. Only at the borders of the data space where only a few cases are located the calculated risks will differ strongly. Here, MMI helps with the comprehensive characterization of uncertainties.

In the context of subjectivity of model selection the following aspect is noted. It would be generally possible to choose a larger number of non-nested plausible models (of the same or similar number of parameters) that could lead to fits of similar shapes. That way one could end up with a situation of having a very large number of models in the set of final non-nested models, each of which with a very small AIC-weight. This situation is prevented by only including into Occam's group those non-nested models with a bilateral AIC-weight larger than 5% (see Table S3 of the Online Resource including the related footnote e).

At low and medium doses our results are in agreement with the earlier findings (Zablotska et al. 2014) and based on a more comprehensive analysis with a larger series of biologically-plausible dose-responses. An essential difference with the primary analysis (Zablotska et al. 2014) is the use of a different baseline model. The present study applied the parametric baseline model given in equation (S4) of the Online Resource with 21 baseline parameters while in (Zablotska et al. 2014) a stratified baseline model with one free parameter for each possible combination of available categories in the data was used. Their baseline model contained several thousand free parameters and was not suitable for AIC-based MMI analysis for which parsimony in parameters is essential (Walsh and Kaiser 2011).

In a recent MMI-based analysis of the LSS mortality data for heart diseases observed during 1950-2003 an *ERR* of 0.08 at 1 Gy with 95% CI: (0, 0.20) was reported (Schöllnberger et al. 2018). Shimizu et al. (2010) reported an *ERR* per dose of 0.14 Gy^{-1} with 95% CI: (0.06, 0.23). Within the error bars these values are consistent with our estimate of 0.216 at 1 Gy with 95% CI: 0.062, 0.48. For IHD, however, these authors did not find a significant association between radiation exposure and IHD (refer to Web Table B in Shimizu et al. 2010). The latest analysis of the LSS mortality data with extended follow-up from 1950-2008 found no significant association between radiation exposure and IHD either (Takahashi et al. 2017). For IHD mortality in male Mayak workers, an *ERR* per dose of 0.09 Gy^{-1} with 95% CI: 0.02, 0.16 was reported (Simonetto et al. 2014). This value is consistent with the risk prediction from the present study. For females, no significant elevation in risk was found (Simonetto et al. 2014). Azizova et al. (2015a) did not find a significant association of total dose from external γ-rays with IHD mortality in Mayak workers. A population-based case-control study of major coronary events (i.e., myocardial infarction, coronary revascularization, or death from ischemic heart diseases) in 2168 women who underwent radiotherapy for breast cancer between 1958 and 2001 in Sweden and Denmark

was conducted by Darby et al. (2013). The study included 963 women with major coronary events and 1205 controls. Rates of major coronary events increased linearly with the mean dose to the heart by 7.4% per gray (95% confidence interval, 2.9 to 14.5; P < 0.001), with no apparent threshold (this corresponds to an ERR per dose of 0,074 with 95% CI: (0,029, 0.145)). Darby and colleagues had applied a linear dose-response model. In that context it is noted that Schneider et al. (2017) put forward arguments that the dose-response may not necessarily be linear. It follows from Darby et al. (2013) that for a mean heart dose of 5 Gy *ERR* = 0.37 with 95% CI: (0.15, 0.73). The value of *ERR* = 0.37 is considerably lower than our MMI estimate for 5 Gy (Table 4: *ERR* = 4.70 at 5 Gy with 95% CI: 0.60, 10). Ghobadi et al. (2012) report results from rodent experiments showing that irradiation of heart, lung, or both independently induces specific cardiac dysfunction and pulmonary vascular damage, mutually enhancing each other. Their findings suggest that irradiation of an already diseased lung can indirectly increase the IHD risk, compared to irradiation of a healthy lung. We may hypothesize that this biological effect increases the IHD risk significantly compared to LNT behavior at doses above 2 Gy, which are concomitantly associated with long duration of tuberculosis.

There remains considerable controversy over the effects of dose protraction on long-term health outcomes. In fact, the ICRP is putting a major effort into evaluating the many modern studies with dose-protraction (Shore et al. 2017). Survivors of atomic bombings in Hiroshima and Nagasaki were exposed to acute exposure and could not provide useful information on the effects of dose-fractionation. Limited data exist on the dose rate effects in Mayak workers, primarily in the form of annual absorbed doses. In contrast, the CFCS has detailed exposure information on the dose and dose rate of a typical fluoroscopic examination and number of fluoroscopic procedures for each patient per year. Altogether, the CFCS is the largest study of patients exposed to moderately fractionated low-to-moderate doses of IR and presents one of the most valuable cohorts worldwide to derive information related to radiation effects at low, moderate and high doses of IR.

For IHD mortality among 308,297 nuclear industry workers from France, United Kingdom and United States, as part of the International Nuclear Workers Study (INWORKS), an *ERR* per dose of 0.18 Sv^{-1} with 90% CI: (0.004, 0.36) was reported (Gillies et al. 2017). Recently, the CFCS data for IHD (Zablotska et al. 2014) were combined with a cohort of tuberculosis fluoroscopy patients from Massachusetts and analyzed with a linear dose-response model applying two different dose regimes with a fixed cut-point at 0.5 Gy (Tran et al. 2017). The authors reported increasing trends for doses <0.5 Gy; over the entire dose range a negative dose trend was observed (Tran et al. 2017). This is probably due to the inability to adjust for dose-fractionation effects in the Massachusetts data where only cumulative doses to the lung have been estimated. The present study used a more comprehensive and flexible approach by analyzing the data with a variety of different linear and non-linear models including those that exhibit flexible threshold-doses without applying artificial cut-points at certain doses and without relying on LNT as a foregone conclusion (Little et al. 2012, Little 2016).

Conclusions

The present study confirms previous findings in a number of studies of essentially linear dose-response for death from IHD at low and moderate doses (0 − 1 Gy). Our analyses suggest that different biological mechanisms may operate at low and medium doses compared to high doses and that at higher doses, the LNT model may underestimate the risk compared to the dose-response from MMI by a factor of 5. Our results should be of particular interest to international radiation protection organizations, which largely rely on analyses of

radio-epidemiological cohorts using the LNT model. We conclude that our findings have important implications for risk assessment of IR in the context of medical applications (such as CT scans and radiotherapy), nuclear energy production and accident related long term risks.

Compliance with ethical standards

Conflict of Interest The authors declare that they have no conflict of interest.

This article does not contain any studies with human participants or animals performed by any of the authors.

References

Akaike H (1973) Information theory and an extension of the maximum likelihood principle. In: Petrov BN, Caski F (ed.). In: Proceedings of the second international symposium on information theory. Akademiai Kiado, Budapest, pp 267–281

Akaike H (1974) A new look at the statistical model identification. IEEE Trans Autom Control 19:716–723

Azizova TV, Grigoryeva ES, Haylock RG, Pikulina MV, Moseeva MB (2015a) Ischaemic heart disease incidence and mortality in an extended cohort of Mayak workers first employed in 1948–1982. Br J Radiol 88:20150169

Azizova TV, Grigorieva ES, Hunter N, Pikulina MV, Moseeva MB (2015b) Risk of mortality from circulatory diseases in Mayak workers cohort following occupational radiation exposure. J Radiol Prot 35:517–538

Brain P, Cousens R (1989) An equation to describe dose responses where there is stimulation of growth at low doses. Weed Res 29:93–96

Burnham KP, Anderson DR (2002) Model selection and multimodel inference, 2nd edn. Springer, New York

Carroll RJ, Ruppert D, Stefanski LA, Crainiceanu CM (2006) Measurement error in nonlinear models: a modern perspective. 2nd edition. Boca Raton, FL: Chapman and Hall/ CRC Monographs on Statistics & Applied Probability

Cedergreen N, Ritz C, Streibig JC (2005) Improved empirical models describing hormesis. Environ Toxicol Chem 24:3166-3172

Claeskens G, Hjort NL (2008) Model selection and model averaging. Cambridge University Press, Cambridge

Darby SC, Cutter DJ, Boerma M, Constine LS, Fajardo LF, Kodama K, Mabuchi K, Marks LB, Mettler FA, Pierce LJ, Trott KR, Yeh ET, Shore RE (2010) Radiation-related heart disease: current knowledge and future prospects. Int J Radiat Oncol Biol Phys 76:656–665

Darby SC, Ewertz M, McGale P, Bennet AM, Blom-Goldman U, Brønnum D, Correa C, Cutter D, Gagliardi G, Gigante B, Jensen MB, Nisbet A, Peto R, Rahimi K, Taylor C, Hall P (2013) Risk of ischemic heart disease in women after radiotherapy for breast cancer. N Engl J Med 368:987–998

Ebrahimian TG, Beugnies L, Surette J, Priest N, Gueguen Y, Gloaguen C, Benderitter M, Jourdain JR, Tack K (2018) Chronic Exposure to External Low-Dose Gamma Radiation Induces an Increase in Anti-inflammatory and Anti-oxidative Parameters Resulting in Atherosclerotic Plaque Size Reduction in ApoE$^{-/-}$ Mice. Radiat Res 189:187-196

Frey B, Hehlgans S, Rödel F, Gaipl US (2015) Modulation of inflammation by low and high doses of ionizing radiation: implications for benign and malign diseases. Cancer Lett 368:230–237

Gillies M, Richardson DB, Cardis E, Daniels RD, O'Hagan JA, Haylock R, Laurier D, Leuraud K, Moissonnier M, Schubauer-Berigan MK, Thierry-Chef I, Kesminiene A (2017) Mortality from circulatory diseases and other non-Cancer outcomes among nuclear workers in France, the United Kingdom and the United States (INWORKS). Radiat Res 188:276–290

Ghobadi G, van der Veen S, Bartelds B, de Boer RA, Dickinson MG, de Jong JR, Faber H, Niemantsverdriet M, Brandenburg S, Berger RM, Langendijk JA, Coppes RP, van Luijk P (2012) Physiological interaction of heart and lung in thoracic irradiation. Int J Radiat Oncol Biol Phys. 84(5):e639-646

Grant EJ, Brenner A, Sugiyama H, Sakata R, Sadakane A, Utada M, Cahoon EK, Milder CM, Soda M, Cullings HM, Preston DL, Mabuchi K, Ozasa K (2017) Solid cancer incidence among the life span study of atomic bomb survivors: 1958–2009. Radiat Res 187:513–537

HPA (2010) Circulatory disease risk. Report of the Independent Advisory Group on Ionising Radiation. Health Protection Agency 2010; ISBN 978-0-85951-676-1

Hoeting JA, Madigan D, Raftery AE, Volinsky CT (1999) Bayesian model averaging: a tutorial. Statist Sci 14:382–417

Hoffmann S, Rage E, Laurier D, Laroche P, Guihenneuc C, Ancelet S (2017) Accounting for Berkson and Classical Measurement Error in Radon Exposure Using a Bayesian Structural Approach in the Analysis of Lung Cancer Mortality in the French Cohort of Uranium Miners. Radiat Res 187(2):196-209

Hoving S, Heeneman S, Gijbels MJ, te Poele JA, Russell NS, Daemen MJ, Stewart FA (2008) Single-dose and fractionated irradiation promote initiation and progression of atherosclerosis and induce an inflammatory plaque phenotype in ApoE$^{-/-}$ mice. Int J Radiat Oncol Biol Phys 71(3):848-857

Howe (1998) Use of computerized record linkage in cohort studies. Epidemiol Rev 20: 112-121

Howe GR, McLaughlin J (1996) Breast cancer mortality between 1950 and 1987 after exposure to fractionated moderate-dose-rate ionizing radiation in the Canadian Fluoroscopy Cohort Study and a comparison with breast cancer mortality in the Atomic Bomb Survivors Study. Radiat Res 145: 694–707

ICRP (2005) Low-dose extrapolation of radiation-related cancer risk. ICRP Publication 99. Ann. ICRP 35(4)

Kaiser JC, Walsh L (2013) Independent analysis of the radiation risk for leukaemia in children and adults with mortality data (1950–2003) of Japanese A-bomb survivors. Radiat Environ Biophys 52:17–27

16

Kreuzer M, Auvinen A, Cardis E, Hall J, Jourdain JR, Laurier D, Little MP, Peters A, Raj K, Russell NS, Tapio S, Zhang W, Gomolka M (2015) Low-dose ionising radiation and cardiovascular diseases--Strategies for molecular epidemiological studies in Europe. Mutat Res Rev Mutat Res 764:90-100

Kreuzer M, Sobotzki C, Schnelzer M, Fenske N (2018) Factors Modifying the Radon-Related Lung Cancer Risk at Low Exposures and Exposure Rates among German Uranium Miners. Radiat Res 189:165-176

Land CE, Kwon D, Hoffman FO, Moroz B, Drozdovitch V, Bouville A, Beck H, Luckyanov N, Weinstock RM, Simon SL (2015) Accounting for shared and unshared dosimetric uncertainties in the dose response for ultrasound-detected thyroid nodules after exposure to radioactive fallout. Radiat Res 183(2):159-173

Le Gallic C, Phalente Y, Manens L, Dublineau I, Benderitter M, Gueguen Y, Lehoux S, Ebrahimian TG (2015) Chronic internal exposure to low dose 137Cs induces positive impact on the stability of atherosclerotic plaques by reducing inflammation in ApoE$^{-/-}$ Mice. PLOS One 10:e0128539

Little MP, Azizova TV, Bazyka D, Bouffler SD, Cardis E, Chekin S, Chumak VV, Cucinotta FA, de Vathaire F, Hall P, Harrison JD, Hildebrandt G, Ivanov V, Kashcheev VV, Klymenko SV, Kreuzer M, Laurent O, Ozasa K, Schneider T, Tapio S, Taylor AM, Tzoulaki I, Vandoolaeghe WL, Wakeford R, Zablotska LB, Zhang W, Lipshultz SE (2012) Systematic review and metaanalysis of circulatory disease from exposure to low-level ionizing radiation and estimates of potential population mortality risks. Environ Health Perspect 120:1503–1511

Little MP, Kukush AG, Masiuk SV, Shklyar S, Carroll RJ, Lubin JH, Kwon D, Brenner AV, Tronko MD, Mabuchi K, Bogdanova TI, Hatch M, Zablotska LB, Tereshchenko VP, Ostroumova E, Bouville AC, Drozdovitch V, Chepurny MI, Kovgan LN, Simon SL, Shpak VM, Likhtarev IA (2014) Impact of uncertainties in exposure assessment on estimates of thyroid cancer risk among Ukrainian children and adolescents exposed from the Chernobyl accident. PLOS One 9(1):e85723

Little MP, Kwon D, Zablotska LB, Brenner AV, Cahoon EK, Rozhko AV, Polyanskaya ON, Minenko VF, Golovanov I, Bouville A, Drozdovitch V (2015) Impact of Uncertainties in Exposure Assessment on Thyroid Cancer Risk among Persons in Belarus Exposed as Children or Adolescents Due to the Chernobyl Accident. PLOS One 10(10):e0139826

Little MP (2016) Radiation and circulatory disease Mutat Res 770(Pt B):299-318

Madigan D, Raftery AE (1994) Model selection and accounting for model uncertainty in graphical models using Occam's window. J Amer Statist Assoc 89:1535–1546

Mancuso M, Pasquali E, Braga-Tanaka I 3rd, Tanaka S, Pannicelli A, Giardullo P, Pazzaglia S, Tapio S, Atkinson MJ, Saran A (2015) Acceleration of atherogenesis in ApoE$^{-/-}$ mice exposed to acute or low-dose-rate ionizing radiation. Oncotarget 6:31263–31271

Mathias D, Mitchel RE, Barclay M, Wyatt H, Bugden M, Priest ND, Whitman SC, Scholz M, Hildebrandt G, Kamprad M, Glasow A (2015) Low-dose irradiation affects expression of inflammatory markers in the heart of ApoE$^{-/-}$ mice. PLOS One 10(3):e0119661

Mitchel RE, Burchart P, Wyatt H (2007) Fractionated, low-dose-rate ionizing radiation exposure and chronic ulcerative dermatitis in normal and Trp53 heterozygous C57BL/6 mice. Radiat Res 168(6):716–724

Mitchel RE, Hasu M, Bugden M, Wyatt H, Little MP, Gola A, Hildebrandt G, Priest ND, Whitman SC (2011) Low-dose radiation exposure and atherosclerosis in ApoE$^{-/-}$ mice. Radiat Res 175:665–676

Mitchel RE, Hasu M, Bugden M, Wyatt H, Hildebrandt G, Chen YX, Priest ND, Whitman SC (2013) Low-dose radiation exposure and protection against atherosclerosis in ApoE$^{-/-}$ mice: the influence of P53 heterozygosity. Radiat Res 179:190–199

Moseeva MB, Azizova TV, Grigoryeva ES, Haylock R (2014) Risks of circulatory diseases among Mayak PA workers with radiation doses estimated using the improved Mayak Worker Dosimetry System 2008. Radiat Environ Biophys 53:469–477

NCRP (2018) Implications of recent epidemiologic studies for the linear nonthreshold model and radiation protection. Commentary No. 27 (Bethesda, MD: National Council on Radiation Protection and Measurements)

Noble RB, Bailer AJ, Park R (2009) Model-averaged benchmark concentration estimates for continuous response data arising from epidemiological studies. Risk Anal 29:558–564

Ozasa K, Shimizu Y, Suyama A, Kasagi F, Soda M, Grant EJ, Sakata R, Sugiyama H, Kodama K (2012) Studies of the mortality of atomic bomb survivors, Report 14, 1950–2003: an overview of cancer and noncancer diseases. Radiat Res 177:229–243

Ozasa K, Takahashi I, Grant EJ, Kodama K (2017) Cardiovascular disease among atomic bomb survivors. Int J Radiat Biol 93(10):1145–1150

Rödel F, Frey B, Gaipl U, Keilholz L, Fournier C, Manda K, Schöllnberger H, Hildebrandt G, Rödel C (2012a) Modulation of inflammatory immune reactions by low-dose ionizing radiation: molecular mechanisms and clinical application. Curr Med Chem 19:1741–1750

Rödel F, Frey B, Manda K, Hildebrandt G, Hehlgans S, Keilholz L, Seegenschmiedt MH, Gaipl US, Rödel C (2012b) Immunomodulatory properties and molecular effects in inflammatory diseases of lowdose x-irradiation. Front Oncol 2:1–9

Schneider U, Ernst M, Hartmann M (2017) The dose-response relationship for cardiovascular disease is not necessarily linear. Radiat Oncol 12:74

Schöllnberger H, Kaiser JC, Jacob P, Walsh L (2012) Dose-responses from multi-model inference for the non-cancer disease mortality of atomic bomb survivors. Radiat Environ Biophys 51:165–178

Schöllnberger H, Eidemüller M, Cullings HM, Simonetto C, Neff F, Kaiser JC (2018) Dose-responses for mortality from cerebrovascular and heart diseases in atomic bomb survivors: 1950-2003. Radiat Environ Biophys 57(1):17-29

Shimizu Y, Kodama K, Nishi N, Kasagi F, Suyama A, Soda M, Grant EJ, Sugiyama H, Sakata R, Moriwaki H, Hayashi M, Konda M, Shore RE (2010) Radiation exposure and circulatory disease risk: Hiroshima and Nagasaki atomic bomb survivor data, 1950–2003. Brit Med J 340:b5349

Shore R, Walsh L, Azizova T, Rühm W (2017) Risk of solid cancer in low dose-rate radiation epidemiological studies and the dose-rate effectiveness factor. Int J Radiat Biol 93:1064-1078

Shore RE, Beck HL, Boice JD Jr , Caffrey EA, Davis S, Grogan HA, Mettler FA Jr, Preston RJ, Till JE, Wakeford R, Walsh L, Dauer LT (2018) Implications of recent epidemiologic studies for the linear nonthreshold model and radiation protection. J Radiol Prot 38:1217-1233

Shore RE, Beck HL, Boice JD Jr , Caffrey EA, Davis S, Grogan HA, Mettler FA Jr, Preston RJ, Till JE, Wakeford R, Walsh L, Dauer LT (2019) Recent epidemiologic studies and the linear no-threshold model for radiation protection - considerations regarding NCRP commentary 27. Health Physics 116: 235-246

Simonetto C, Azizova TV, Grigoryeva ES, Kaiser JC, Schöllnberger H, Eidemüller M (2014) Ischemic heart disease in workers at Mayak PA: latency of incidence risk after radiation exposure. PLOS One 9:e96309

Simonetto C, Schöllnberger H, Azizova TV, Grigoryeva ES, Pikulina MV, Eidemüller M (2015) Cerebrovascular diseases in workers at Mayak PA: The Difference in Radiation Risk between Incidence and Mortality. PLOS ONE 10:e0125904

Stewart FA, Heeneman S, Te Poele J, Kruse J, Russell NS, Gijbels M, Daemen M (2006) Ionizing radiation accelerates the development of atherosclerotic lesions in ApoE$^{-/-}$ mice and predisposes to an inflammatory plaque phenotype prone to hemorrhage. Am J Pathol 168:649-658

Takahashi I, Shimizu Y, Grant EJ, Cologne J, Ozasa K, Kodama K (2017) Heart disease mortality in the Life Span Study, 1950–2008. Radiat Res 187:319–332

Tran V, Zablotska LB, Brenner AV, Little MP (2017) Radiation-associated circulatory disease mortality in a pooled analysis of 77,275 patients from the Massachusetts and Canadian tuberculosis fluoroscopy cohorts. Sci Rep 7:44147

UNSCEAR (2000) Sources and Effects of Ionizing Radiation. United Nations Scientific Committee on the Effects of Atomic Radiation. UNSCEAR 2000 Report to the General Assembly, with scientific annexes. Volume II: Effects
http://www.unscear.org/docs/publications/2000/UNSCEAR_2000_Report_Vol.II.pdf

Walsh L (2007) A short review of model selection techniques for radiation epidemiology. Radiat Environ Biophys 46:205–213

Walsh L, Kaiser JC (2011) Multi-model inference of adult and childhood leukaemia excess relative risks based on the Japanese A-bomb survivors mortality data (1950–2000). Radiat Environ Biophys 50:21–35

Williams LK, Csaki LS, Cantor RM, Reue K, Lawson GW (2012) Ulcerative dermatitis in C57BL/6 mice exhibits an oxidative stress response consistent with normal wound healing. Comp Med 62(3):166-171

World Health Organization (2013) The top 10 causes of death. http://who.int/mediacentre/factsheets/fs310/en/index.html

Yusuf S, Hawken S, Ounpuu S, Dans T, Avezum A, Lanas F, McQueen M, Budaj A, Pais P, Varigos J, Lisheng L; INTERHEART Study Investigators (2004) Effect of potentially modifiable risk factors associated with myocardial infarction in 52 countries (the INTERHEART study): case-control study. Lancet 364:937-952

Zablotska LB, Little MP, Cornett RJ (2014) Potential increased risk of ischemic heart disease mortality with significant dose fractionation in the Canadian Fluoroscopy Cohort Study. Am J Epidemiol 179(1):120-131

Figure legends

Fig. 1 Typical shapes of the functions that were used to analyze the dose-response for IHD mortality in the Canadian Fluoroscopy Cohort Study (follow-up 1950–1987). 1st row: linear no-threshold (LNT) model, quadratic (Q), linear-quadratic (LQ); 2nd row: linear-exponential (LE) model, linear threshold (LTH), smooth step model; 3rd row: sigmoid model, hormesis model, two-line spline model; 4th row: Gompertz model, categorical model. Additional dashed lines show the flexibility of some of the models

Fig. 2 *ERR* for IHD mortality in the Canadian Fluoroscopy Cohort Study (follow-up 1950–1987) versus cumulative lagged lung dose for the four final non-nested ERR models (Table 3) and the simulated dose-response curves from MMI, calculated with the sparse model approach and the rich model approach. The shaded area represents the 95% CI region for the MMI (sparse model approach). For AIC-weights see the insert. The dotted straight line shows the risk prediction from (Zablotska et al. 2014). The ERR-LNT model from the present study and the LNT model from Zablotska et al. (2014) give almost identical risk predictions. The figure is valid for males and females. A dose-fractionation of 0.2 Gy yr^{-1} was assumed. Point estimates and related 95% CI from the fit of an ERR-categorical model that divides the dose range into the following categories ($D < 10^{-6}$ Gy, 10^{-6} Gy $\leq D < 1$ Gy; 1 Gy $\leq D < 2$ Gy, 2 Gy $\leq D < 6$ Gy, and $D \geq 6$ Gy) are as follows: *ERR* = 0.0089 (–0.0173; 0.0348), *ERR* = 0.1820 (–0.0652; 0.428), *ERR* = 1.002 (–0.225; 2.23), *ERR* = 10.3 (–17.8; 38.1). In the categorical fit, zero risk was assigned to the dose range $D < 10^{-6}$ Gy. The point estimates and their 95% CI are not shown in the figure because of the very large 95% CI for the highest dose category. Online version contains color

Fig. 3 *ERR* for IHD mortality in the Canadian Fluoroscopy Cohort Study (follow-up 1950–1987) versus cumulative lagged lung dose up to 2 Gy for the four final non-nested ERR models (Table 3) and the simulated dose-response curves from MMI, calculated with the sparse model approach and the rich model approach. Vertical dotted lines represent the 95% CI region for the MMI (sparse model approach). For AIC-weights see the insert. The dotted straight line shows the risk prediction from (Zablotska et al. 2014). The figure is valid for males and females. A dose-fractionation of 0.2 Gy yr^{-1} was assumed. Online version contains color

Fig. 4 *ERR* for IHD mortality in the Canadian Fluoroscopy Cohort Study (follow-up 1950–1987) versus cumulative lagged lung dose up to 0.1 Gy for the four final non-nested ERR models (Table 3) and the simulated dose-response curves from MMI, calculated with the sparse model approach and the rich model approach. Vertical dotted lines represent the 95% CI region for the MMI (sparse model approach). For AIC-weights see the insert. The dotted straight line shows the risk prediction from (Zablotska et al. 2014). The figure is valid for males and females. A dose-fractionation of 0.2 Gy yr^{-1} was assumed. Online version contains color

21

Electronic Supplementary Material

The Online Resource provides in Table S1 characteristics of the Canadian Fluoroscopy Cohort Study Data. Subsequently, the baseline model from Simonetto et al. (2014) that had been developed for the Mayak workers cohort is presented. This is followed by the baseline model applied in the present study. Page 7 gives the mathematical form of all dose-response models that were tested in the present study. The next section provides a detailed explanation how the AIC-weights are calculated for both, the sparse and rich model approaches. It supplies an equation that was used to calculate the normalized AIC-weights given in Table 3 (main text). Page 10 contains the section "Software" and gives a brief introduction to the software package used for the analyses. Figure S1 provides the number of model parameters for the applied dose-response models and relation between the models regarding their nestedness. Table S2 supplies model parameters (baseline and radiation-associated), maximum likelihood estimates and Wald-type standard errors for the four final non-nested models that were used for MMI (sparse model approach). The next section gives a detailed description of how the model selection was performed according to the sparse model approach. This is followed by Table S3 on page 17. This table is an extension of Table 3 (main text) and provides the results of fitting the dose-response models from Figure 1 as ERR models to the CFCS data. Among other information, the final deviance values are provided together with the AIC-values, normalized and bilateral AIC-weights. All of this information is given for the sparse and the rich model approaches. Figure S2 shows the baseline cases as predicted by the ERR-LNT model versus attained age with the secular trend together with crude rates. The references are provided on page 21.

Figure 1
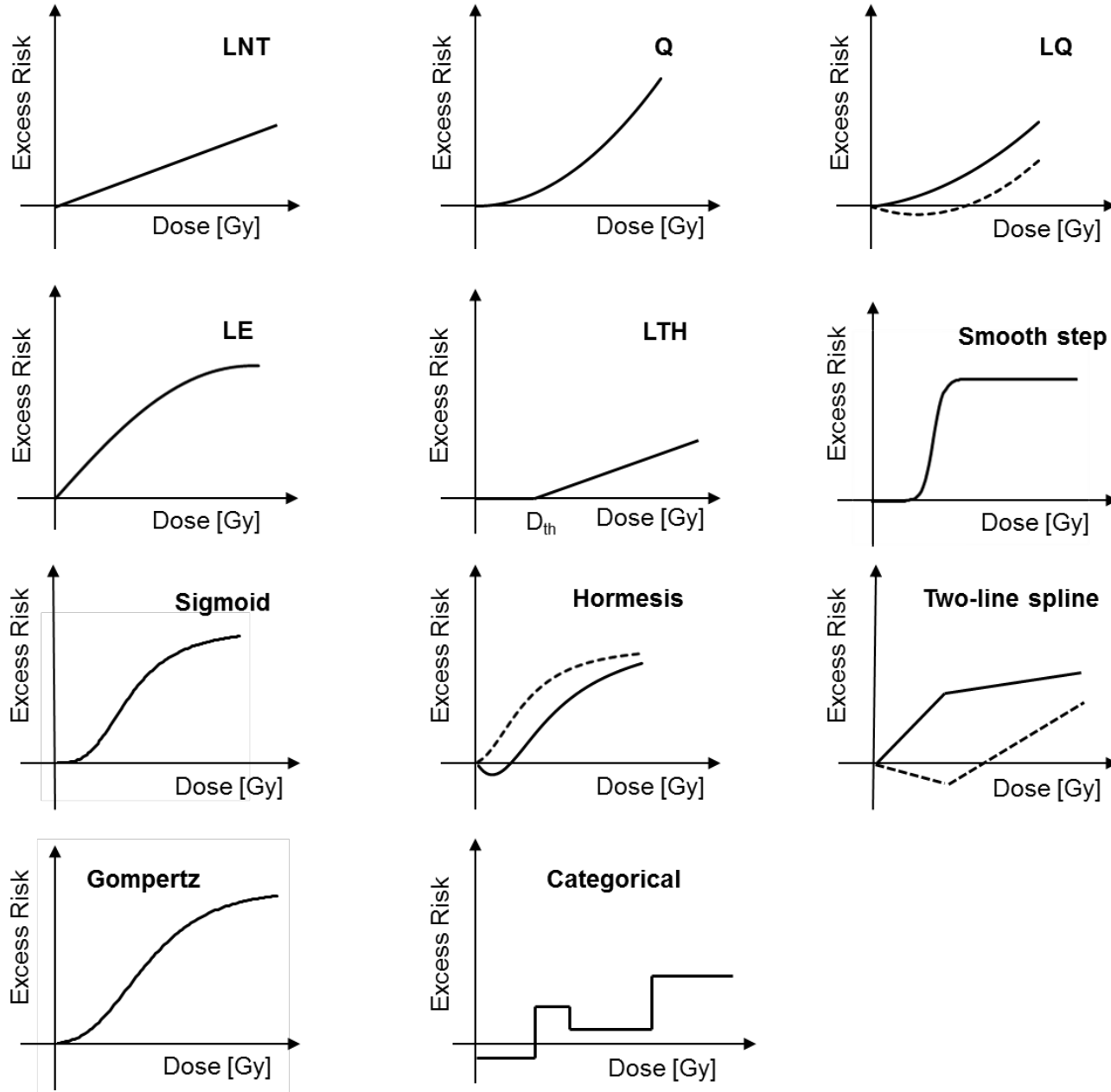
Figure 1

Figure 2

Figure 2
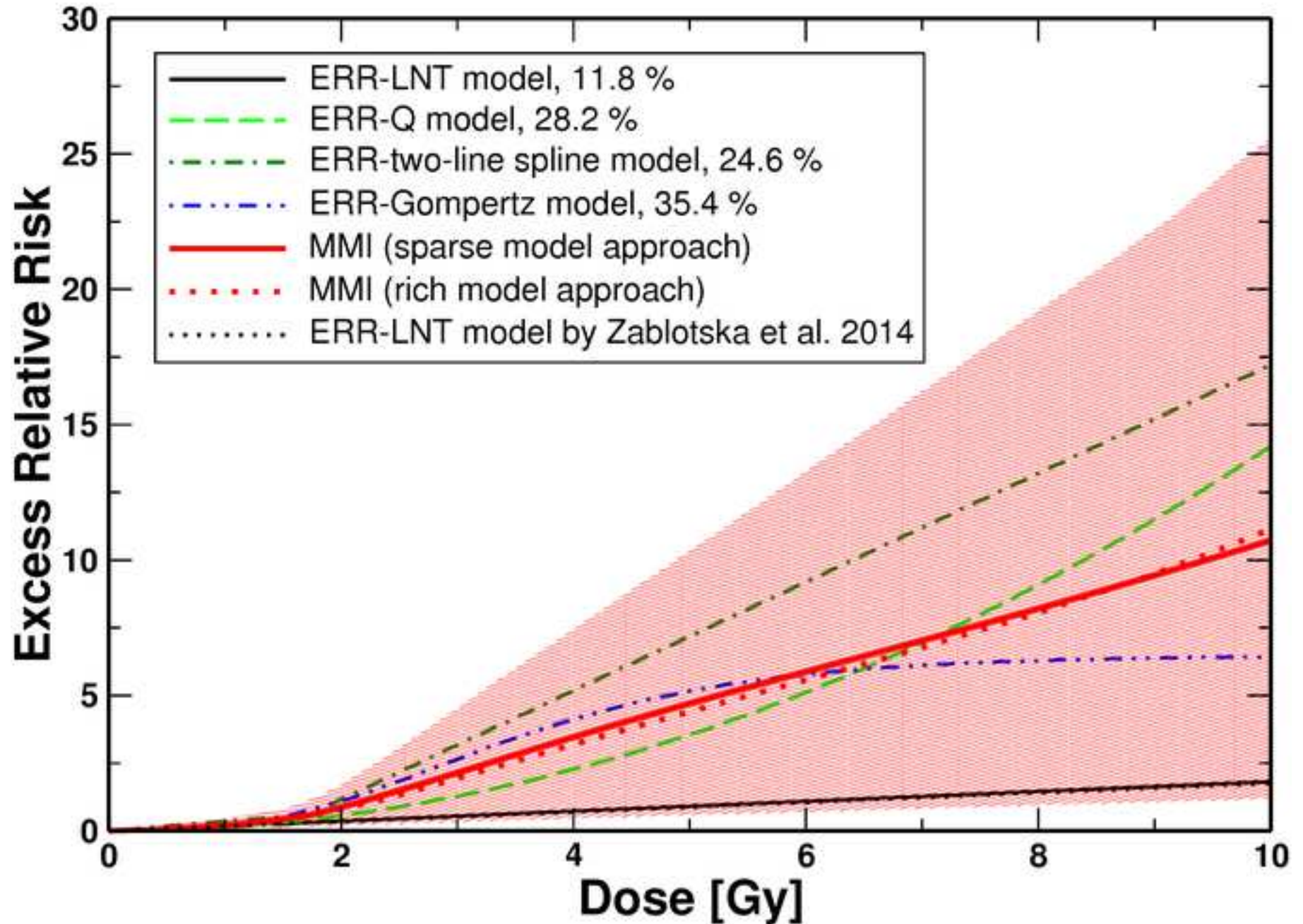
Figure 3
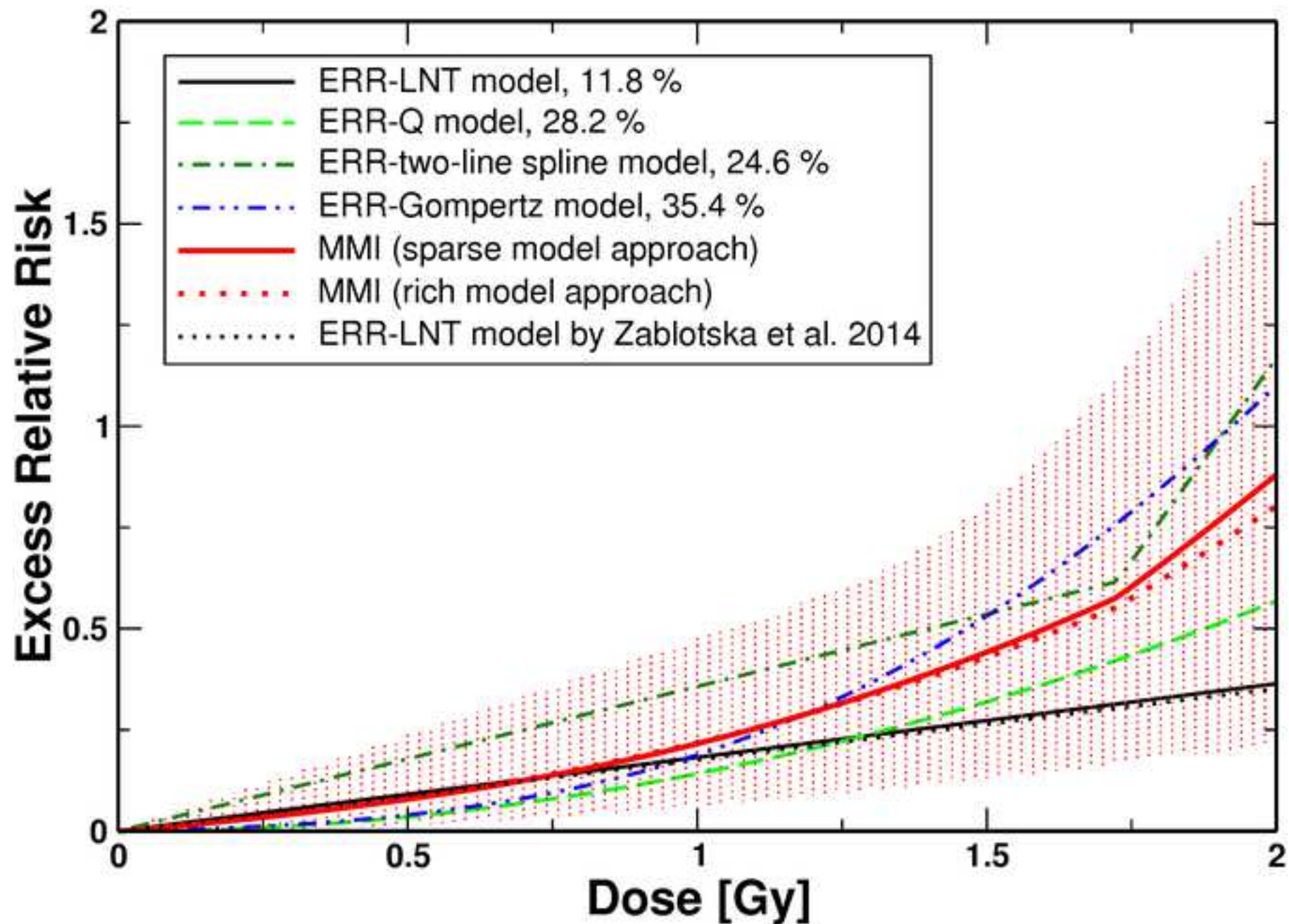
Figure 3

Figure 4

Figure 4
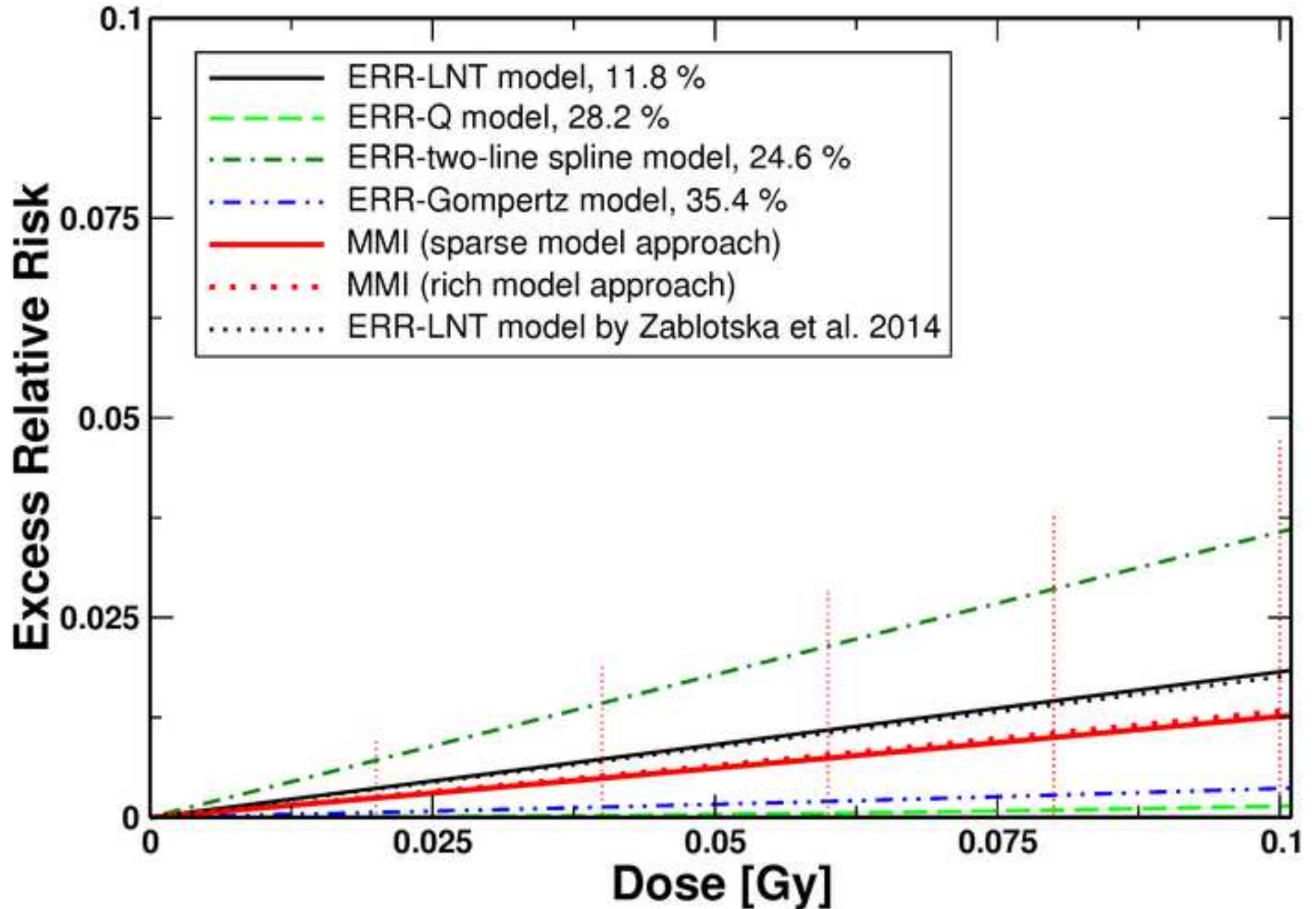
Table 1 Dose-response models used for MMI and related biological studies that motivate the use of these specific models in the present study; Canadian Fluoroscopy Cohort Study, 1950-1987

err(*D*)	Name of model	Biological outcome and dose type investigated	References
$\beta_1 \times D$	LNT	Number of carotid artery lesions per animal, plaque area and inflammatory content of carotid artery lesions in ApoE$^{-/-}$ mice; 0 or 14 Gy of X-rays see Q model	Stewart et al. (2006) Hoving et al. (2008)
$\beta_1 \times D^2$	Q	Number of atherosclerotic lesions in carotid arteries per animal, plaque area and plaque phenotype in ApoE$^{-/-}$ mice; 0, 8 Gy or 14 Gy of X-rays	Hoving et al. (2008)[a]
$\beta_1 \times D + \beta_2 \times D^2$	LQ[b]	see Q model see hormesis model see hormesis model see hormesis model see LE model	Hoving et al. (2008) Mitchel et al. (2011) Mitchel et al. (2013) Ebrahimian et al. (2018) Mancuso et al. (2015)
$\beta_1 \times D \times \exp(\beta_2 D)$	LE	Atherosclerotic features (plaque density, plaque size and plaque vulnerability) in ApoE$^{-/-}$ mice; acute irradiation with single doses of 0.3 or 6 Gy X-rays at 0.89 Gy min^{-1}; low dose rate exposures with ^{137}Cs γ-rays (22 hr day^{-1}) yielding cumulative total doses of 0.3 or 6 Gy in 300 days (dose rate of 1 mGy day^{-1} or 20 mGy day^{-1}, respectively)	Mancuso et al. (2015)

Table 1 continued

$err(D)$	Name of model	Biological outcome and dose type investigated	References
$\begin{cases} 0 & \text{for } D < D_{th} \\ \beta_1 \times (D - D_{th}) & \text{for } D \geq D_{th} \end{cases}$	LTH	Disease frequency and severity of chronic ulcerative dermatitis in *Trp53* normal (*Trp53*$^{+/+}$) or heterozygous (*Trp53*$^{+/-}$) female C57BL/6 mice; fractionated low-dose and low-dose rate ^{60}Co γ-radiation (0.33 mGy per day delivered at 0.7 mGy hr^{-1}; 5 days week^{-1}; for 30 weeks, 60 weeks or 90 weeks yielding 48 mGy, 97 mGy or 146 mGy, respectively	Mitchel et al. (2007)
		see hormesis model see hormesis model see hormesis model	Mitchel et al. (2011) Mitchel et al. (2013) Ebrahimian et al. (2018)
		Inflammatory and thrombotic markers in the heart of ApoE$^{-/-}$ mice; total body irradiation (^{60}Co γ-irradiation) with 0.025, 0.05, 0.1, 0.5 or 2 Gy at low (1 mGy min^{-1}) or high dose rate (150 mGy min^{-1})	Mathias et al. (2015)
		Atherosclerotic features (plaque size and phenotype, plaque inflammatory profile and oxidative stress status) in ApoE$^{-/-}$ mice; chronic internal exposure to ^{137}Cs via drinking water; the resulting absorbed doses were 3, 15, and 75 mGy after 6 months and 6, 30, and 150 mGy after 9 months exposure to 4, 20 and 100 kBq l^{-1} of ^{137}Cs, respectively	Le Gallic et al. (2015)

Table 1 continued

$err(D)$	Name of model	Biological outcome and dose type investigated	References
$0.5 \times scale \times [\tanh(s\,(D - D_{th})) - \tanh(-s\,D_{th})]$	Smooth step	see LTH model	Mitchel et al. (2007)
		see LTH model	Mathias et al. (2015)
		see LTH model	Le Gallic et al. (2015)
		see hormesis model	Mitchel et al. (2011)
		see hormesis model	Mitchel et al. (2013)
		see hormesis model	Ebrahimian et al. (2018)
		see LE model	Mancuso et al. (2015)
$\lambda_0 \left(1 - \dfrac{1}{1 + \left(\dfrac{D}{D_{th}} \right)^{\lambda_1}} \right)$	Sigmoid[c]	see LTH model	Mitchel et al. (2007)
		see LTH model	Mathias et al. (2015)
		see LTH model	Le Gallic et al. (2015)
		see hormesis model	Mitchel et al. (2011)
		see hormesis model	Mitchel et al. (2013)
		see hormesis model	Ebrahimian et al. (2018)
		see LE model	Mancuso et al. (2015)

Table 1 continued

$err(D)$	Name of model	Biological outcome and dose type investigated	References
$$\lambda_0 - \frac{\lambda_0 + \lambda_2 D}{1 + \left(\dfrac{D}{D_{th}}\right)^{\lambda_1}}$$	Hormesis[d]	Atherosclerotic features (aortic lesion frequency, size and severity, total serum cholesterol levels and the uptake of lesion lipids by lesion-associated macrophages) in ApoE$^{-/-}$ mice; 0, 0.025, 0.05, 0.10 or 0.50 Gy ^{60}Co γ-irradiation at either low dose rate (1.0 mGy min^{-1}) or high dose rate (app. 0.15 Gy min^{-1})	Mitchel et al. (2011)
		Atherosclerotic features (aortic lesion frequency, size and severity, total serum cholesterol levels) in ApoE$^{-/-}$ mice with reduced *p53* function (*Trp53*$^{+/-}$); 0, 0.025, 0.05, 0.10 or 0.50 Gy ^{60}Co γ-irradiation at either low dose rate (1.0 mGy min^{-1}) or high dose rate (app. 0.15 Gy min^{-1})	Mitchel et al. (2013)
		Atherosclerotic development (plaque size and phenotype, inflammatory profile and oxidative stress status) in ApoE$^{-/-}$ mice; chronic γ-irradiation for 8 months at 12 or 28 μGy hr^{-1}, yielding cumulative doses of 67 and 157 mGy, respectively	Ebrahimian et al. (2018)

Table 1 continued

$err(D)$	Name of model	Biological outcome and dose type investigated	References
$\begin{cases}\beta_1 \times D & \text{for } D < D_{th} \\ \beta_1 \times D_{th} + \beta_2 \times (D - D_{th}) & \text{for } D \geq D_{th}\end{cases}$	Two-line spline[e]	see LNT model	Stewart et al. (2006)
		see LNT model	Hoving et al. (2008)
		see LTH model	Mitchel et al. (2007)
		see LTH model	Mathias et al. (2015)
		see LTH model	Le Gallic et al. (2015)
		see hormesis model	Mitchel et al. (2011)
		see hormesis model	Mitchel et al. (2013)
		see hormesis model	Ebrahimian et al. (2018)
		see LE model	Mancuso et al. (2015)
$\beta_1 \times \exp\{-\beta_2 \exp[-\beta_3 \times (D - D_{th})]\} -$ $\beta_1 \times \exp\{-\beta_2 \exp[-\beta_3 \times (-D_{th})]\}$	Gompertz[f]	see LNT model	Stewart et al. (2006)
		see LQ model	Hoving et al. (2008)
		see LTH model	Mitchel et al. (2007)
		see LTH model	Mitchel et al. (2011)
		see LTH model	Mitchel et al. (2013)
		see LTH model	Mathias et al. (2015)
		see LTH model	Le Gallic et al. (2015)
		see LTH model	Ebrahimian et al. (2018)
		see LE model	Mancuso et al. (2015)

[a] The publication by Hoving et al. (2008) shows that female mice 30 weeks after a 14 Gy exposure exhibited a higher number of initial atherosclerotic lesions per animal compared to a linear extrapolation from the number of lesions obtained after 8 Gy (Figure 3, panel B). Panel E of Figure 3 in Hoving et al. (2008) shows a similar result for the mean of the individual plaque area for initial lesions in female mice 30 weeks after exposure. These findings exhibit a quadratic or linear-quadratic dose-response.

[b] The LQ model has the capability to describe shallow U-shaped or J-shaped dose-responses (Figure 1). Therefore, in addition to the reference Hoving et al. (2008), which gives support for the use of quadratic or linear-quadratic dose-response models, the same references are provided as for the hormesis model. In addition, the LQ model can describe supralinear dose-responses. Consequently, the reference Mancuso et al. (2015) is also listed in this context.

[c] The sigmoid model can exhibit similar shapes as the smooth step model. Therefore, the same references are relevant as for the smooth step model.

[d] This empirical hormesis model has been introduced by Brain and Cousens (1989) to describe stimulation of plant growth after low-dose herbicide exposures. Some adaptations to the model by Brain and Cousens (1989) have been made by Cedergreen et al. (2005) and Simonetto et al. (2014) to yield the specific mathematical form applied in the present study.

[e] The two-line spline model was applied because of its capability to describe supralinear or sublinear dose-responses (Figure 1). Therefore, the same references are provided as for the LE, LTH and hormesis models. Because it can also describe LNT dose-responses, the references Stewart et al. (2006) and Hoving et al. (2008) were added.

[f] The Gompertz model is very flexible and can exhibit linear no-threshold dose-responses, sublinear and smooth step responses but also supralinear dose-responses. Therefore, its use in the present study is motivated by the same biological findings referenced in the context of the LNT model, the linear-quadratic, LTH, smooth step and linear-exponential models.

table 2   Click here to access/download;table;Table 2.doc ✉

Table 2 Maximum likelihood estimates of model parameters, related 95% confidence intervals and final deviances of fitting ERR-LNT models to the mortality data for ischemic heart diseases (Zablotska et al. 2014); Canadian Fluoroscopy Cohort Study, 1950-1987

Parameter	Zablotska et al. (2014), LNT model without dose-fractionation adjustment[a]	Zablotska et al. (2014), LNT model with dose-fractionation adjustment[a]	Present study, LNT model without dose-fractionation adjustment[a,b]	Present study, LNT model with dose-fractionation adjustment[a,c,d]
β_1	0.007 Gy^{-1} (−0.044, 0.072)	0.176 Gy^{-1} (0.011, 0.39)	−0.046 Gy^{-1} (−0.075, −0.013)	0.182 Gy^{-1} (0.049, 0.33)
β_2		−10.2 years Gy^{-1} (−25, −2.1)		−12.0 years Gy^{-1} (−21, −5.1)
dev	9884.50	9879.76	13250.95	13247.75

Abbreviations: dev, final deviance; ERR-LNT, linear no-threshold model implemented as excess relative risk model.

[a] The difference between the model applied by Zablotska et al. (2014) and the one from the present study is the baseline model (stratified in the first case, parametric in the present study; see Web Appendix 5).

[b] Fit was performed with model given in equation (1) with $\beta_2 = 0$.

[c] Fit was performed with model given in equation (1).

[d] As a comparison, the fit of the parametric baseline model alone with its 21 parameters led to dev = 13252.68.

Table 3 Results of fitting the dose-response models from Figure 1 as ERR models to the mortality data for ischemic heart diseases (Zablotska et al. 2014); Canadian Fluoroscopy Cohort Study, 1950-1987

	dev[a]	Δdev[b]	N_{par}	AIC[c]	ΔAIC[d]	Normalized AIC-weights, sparse model approach[e]	Normalized AIC-weights, rich model approach[f]
ERR-LNT	13247.75	6.19	23	13293.75	2.19	0.1183	0.0776
ERR-Q	13246.01	4.46	23	13292.01	0.46	0.2815	0.1847
ERR-LQ	13245.38	3.83	24	13293.38	1.83		0.0930
ERR-LE	13245.68	4.13	24	13293.68	2.13		0.0802
ERR-LTH, $D_{th} = 0.58$ Gy	13246.81	5.26	24	13294.81	3.26		0.0455
ERR-smooth step, $D_{th} = 4,47$ Gy	13244.45	2.90	25	13294.45	2.90		0.0546
ERR-sigmoid, $D_{th} = 41,53$ Gy	13245.94	4.39	25	13295.94	4.39		0.0259
ERR-hormesis, $D_{th} = 3,28$ Gy	13242.84	1.29	26	13294.84	3.29		0.0449
ERR-two-line spline, $D_{th} = 1.72$ Gy	13242.28	0.73	25	13292.28	0.73	0.2461	0.1615
ERR-Gompertz, $D_{th} = 0$	13241.55	0	25	13291.55	0	0.3541	0.2323
ERR-categorical	13242.19	0.63	29	13300.19	8.63		

Abbreviations: AIC, Akaike Information Criterion; dev, final deviance; ERR-LNT, linear no-threshold model implemented as excess relative risk model; ERR-Q, quadratic model implemented as excess relative risk model; ERR-LQ, linear-quadratic model implemented as excess relative risk model; ERR-LE, linear-exponential model implemented as excess relative risk model; ERR-LTH, linear-threshold model implemented as excess relative risk model.

[a] As a comparison, the fit of the baseline model alone with its 21 parameters led to dev = 13252.68.

[b] The difference in final deviance is denoted by Δdev with respect to the model with the smallest final deviance.

[c] AIC = dev + 2 × N_{par}, where N_{par} is the number of model parameters.

[d] The difference in AIC-values with respect to the model with the smallest AIC-values is denoted by ΔAIC.

[e] According to the sparse model approach four models survive the selection process and are used for MMI. The normalized AIC-weights provided here were calculated with equation (S5) from Web Appendix 4.

[f] According to the rich model approach all models except the categorical model survive the selection process because when compared to the model with ΔAIC = 0 they have an AIC-weight > 0.05 (see Table S3 of the Online Resource). The normalized AIC-weights provided here were calculated with equation (S5) from Web Appendix 4.

table 4   Click here to access/download;table;Table 4.doc ⬇

Table 4 Values for *ERR* for mortality from ischemic heart diseases (Zablotska et al. 2014) at various cumulative lung doses calculated with MMI (sparse model approach) and the four final non-nested models; Canadian Fluoroscopy Cohort Study, 1950-1987

Lung dose (Gy)	MMI[a,b]	ERR-LNT model[b,c]	ERR-Q model[b]	ERR-two-line spline[b]	ERR-Gompertz[b]
0.1	0.01263 (0.00075; 0.048)	0.0182 (0.0045; 0.032)	0.0014 (0.00049; 0.0024)	0.036 (0.017; 0.054)	0.0036 (0.0013; 0.0060)
0.2	0.0266 (0.0028; 0.095)	0.0364 (0.0089; 0.064)	0.0057 (0.0020; 0.0094)	0.071 (0.035; 0.11)	0.0089 (0.0033; 0.015)
0.5	0.079 (0.016; 0.24)	0.091 (0.022; 0.16)	0.036 (0.012; 0.059)	0.179 (0.087; 0.27)	0.040 (0.015; 0.066)
1	0.216 (0.062; 0.48)	0.182 (0.045; 0.32)	0.142 (0.049; 0.24)	0.36 (0.17; 0.54)	0.188 (0.070; 0.31)
2	0.88 (0.21; 1.7)	0.364 (0.089; 0.64)	0.57 (0.20; 0.94)	1.17 (0.64; 1.7)	1.1 (0.41; 1.8)
5	4.70 (0.60; 10)	0.91 (0.22; 1.6)	3.6 (1.2; 5.9)	7.2 (2.3; 12)	5.2 (1.9; 8.5)
10	11 (1.2; 26)	1.82 (0.45; 3.2)	14.2 (4.9; 24)	17.2 (4.8; 30)	6.4 (2.4; 11)

Abbreviations: ERR-LNT, linear no-threshold model implemented as excess relative risk model; ERR-Q, quadratic model implemented as excess relative risk model; MMI, multi-model inference.

[a] Calculated with the sparse model approach.

[b] 95% CI are provided in parenthesis.

[c] As a comparison, the *ERR* per dose from Zablotska et al. (2014) is 0.176 Gy^{-1} with 95% CI: 0.011, 0.393.

table 5   Click here to access/download;table;Table 5.doc ⬇

Table 5 Radiation-associated excess cases for the mortality data for ischemic heart diseases (Zablotska et al. 2014) according to the four final non-nested models and MMI (sparse model approach); Canadian Fluoroscopy Cohort Study, 1950-1987

Dose-bin	MMI[a]	ERR-LNT	ERR-Q	ERR-two-line spline	ERR-Gompertz
0 - 0.05 Gy	2.8	5.7	0.2	7.4	0.6
0.05 - 0.1 Gy	1.1	2	0.2	2.7	0.3
0.1 - 0.2 Gy	1.3	2.2	0.3	3.3	0.3
0.2 - 0.3 Gy	2.8	4	0.8	7.5	0.7
0.3 - 0.4 Gy	2.6	3.8	1.1	6.4	0.7
0.4 - 0.5 Gy	3.6	4.8	1.8	8.4	1.4
0.5 - 0.75 Gy	8.9	10	4.6	20.2	4
0.75 - 1 Gy	11.5	11.7	7.2	23.1	6.9
1 - 1.5 Gy	19.7	15.6	12.3	33.9	17
1.5 - 2 Gy	14	8.9	9.4	19.9	15.2
2 - 3 Gy	18	6.2	8.2	32.6	19.7
3 - 4 Gy	7.8	2	3.8	13.3	9.1
4 - 5 Gy	3.3	0.7	1.7	5.4	3.9
5 Gy -	4.7	1.1	3.6	7.3	5
sum:	102.1	78.7	55.2	191.4	84.8

Abbreviations: ERR-LNT, linear no-threshold model implemented as excess relative risk model; ERR-Q, quadratic model implemented as excess relative risk model; MMI, multi-model inference.

[a] Calculated with the sparse model approach.

Supplementary Material

Radio-biologically Motivated Modeling of Radiation Risks of Mortality From Ischemic Heart Diseases in the Canadian Fluoroscopy Cohort Study

Radiation and Environmental Biophysics

Helmut Schöllnberger, Jan Christian Kaiser, Markus Eidemüller, Lydia B. Zablotska

Helmut Schöllnberger (✉)
Helmholtz Zentrum München
Department of Radiation Sciences
Institute of Radiation Medicine
Ingolstädter Landstrasse 1
D-85764 Neuherberg
Germany
schoellnberger@helmholtz-muenchen.de

Federal Office for Radiation Protection
Division UR - Environmental Radioactivity
Ingolstädter Landstrasse 1
D-85764 Neuherberg
Germany
Phone: +49 (0)30-18333-2522
Fax: +49 (0)30-18333-2205
hschoellnberger@bfs.de

Table of Contents

Table S1 Characteristics of the Canadian Fluoroscopy Cohort Study Data (n=63,707), 1950-1987 (Zablotska et al. 2014)

Characteristic	No.	Mean	Median	Range
Person-years of follow-up	1,902,252			
Follow-up, years		31		0-37
Age at end of follow-up, years		65		1-99
Time since first exposure, years		39		0-57
Number of fluoroscopic procedures[a]			64	1-2041
Duration of fluoroscopy screenings, years[a]			2	0-35
Dose fractionation, Gy yr^{-1} [a]			0.36	0-7.30
Total dose, Gy[b]		0.79		0-11.60

All values within this table were taken from Table 1 in Zablotska et al. (2014).

[a] Exposed subjects only.

[b] Cumulative person-time-weighted lung dose.

Baseline model of Simonetto et al. (2014) developed for the Mayak workers cohort

$$h_0 = 10^{-5} \times e^{\psi_{cat} + \psi_{time} + \psi_{emigration}}$$

$$\psi_{cat} = \psi_{smoking} + \psi_{drinking} + \psi_{bmi} + \psi_{blood\,pressure} + \psi_{plant}$$

$$\psi_{time} = \psi_{age} + \psi_{birth} + \psi_{calendar} + \psi_{employment}$$

$$\psi_{emigration} = \varepsilon \times \Theta(b + a - m)$$

$$\psi_{age} = \psi_0 + \psi_1 \ln\left(\frac{a}{60}\right) + \psi_2 \ln^2\left(\frac{a}{60}\right) + \sum_i \alpha_i \ln^2\left(\frac{a}{\vartheta_{\alpha,i}}\right)\Theta(a - \vartheta_{\alpha,i})$$

$$\psi_{birth} = \beta_1 \frac{b - 1900}{10} + \beta_2 \frac{(b - 1900)^2}{100}$$

$$\psi_{calendar} = \sum_i \gamma_i \frac{LT(b + a - \vartheta_{\gamma,i})}{10} \tag{S1}$$

$$\psi_{employment} = \delta_1 \frac{f - 1950}{10} + \delta_2 \frac{(f - 1950)^2}{100}$$

Here, h_0 is the baseline hazard, referred to in the main text as parametric baseline model. Summands in ψ_{cat} evaluate to zero for non-smoker, non-drinker, for persons with normal body mass index, normal blood pressure and for reactor workers. Otherwise they evaluate to some value determined by the fit. The lower case Greek symbols are free parameters. The quantities a, b, f and m denote attained age, birth date, date of first employment at Mayak Production Association (PA) and date of emigration from Ozyorsk, the closed city in which the Mayak workers have lived throughout the operation of the Mayak PA. The quantities $\vartheta_{\alpha,i}$ and $\vartheta_{\gamma,i}$ denote so called age knots. Furthermore, the Heaviside step function Θ was applied together with a function $LT(t)$:

$$\Theta(t) = \begin{cases} 0 & \text{for } t < 0 \\ 1 & \text{for } t \geq 0 \end{cases} \qquad\qquad LT(t) = \begin{cases} 0 & \text{for } t < 0 \\ t & \text{for } t \geq 0 \end{cases} \tag{S2}$$

For some further explanations the reader is referred to the Appendix in Simonetto et al. (2014).

Baseline model applied in the present study

The parametric baseline model that was applied in the present study is as follows.

$$h_0 = 10^{-4} \times e^{\psi_{cat} + \psi_{time}}$$

$$\psi_{cat} = \psi_{gender} + \psi_{province} + \psi_{duration} + \psi_{diagnosis} + \psi_{stage}$$

$$\psi_{time} = \psi_{age} + \psi_{birth} \tag{S3}$$

$$\psi_{age} = \psi_1 \ln(\frac{a}{50}) + \sum_i \alpha_i \ln^2(\frac{a}{\vartheta_{\alpha,i}})\Theta(a - \vartheta_{\alpha,i})$$

$$\psi_{birth} = \beta_1 \frac{b - 1900}{10} + \beta_2 \frac{(b - 1900)^2}{100}$$

For all parameters a distinction according to sex was allowed for. The actual baseline model that was fitted to the CFCS data in the present study is as follows:

$$
\begin{aligned}
h_0 = 10^{-4} \times \exp\{ & c\_m + c\_f + prov\_m + prov\_f + cdur\_m + cdur\_f + \\
& diag\_m + diag\_f + nostg\_m + nostg\_f + \\
& stg1\_m + stg1\_f + stg2\_m + stg2\_f + stg3\_m + stg3\_f + \\
& ba\_m \times \ln(a/50) + ba\_f \times \ln(a/50) + \\
& basq\_m \times \ln^2(a/50) \times \Theta(a-50) + basq\_f \times \ln^2(a/50) \times \Theta(a-50) + \\
& bb\_m \times ((b-1900)/10) + bb\_f \times ((b-1900)/10) + \\
& bbsq\_m \times ((b-1900)^2/100) + bbsq\_f \times ((b-1900)^2/100) \}
\end{aligned}
\tag{S4}
$$

Model parameters in equation (S4) are italicised. The free parameters c_m and c_f relate to males and females, respectively. The free parameters $prov\_m$ and $prov\_f$ relate to males and females admitted to hospitals outside the Canadian province of Nova Scotia, respectively. The parameters $cdur\_m$ and $cdur\_f$ are associated with duration of fluoroscopy screenings in male and female patients, respectively. The parameters $diag\_m$ and $diag\_f$ relate to males and females with diagnosis pulmonary tuberculosis, respectively. Furthermore, $nostg\_m$ relates to male patients who - related to the stage of tuberculosis - contain the status not assigned (i.e. not specified). The parameter $stg3\_f$ is associated with females with advanced stage of tuberculosis. The free parameter ba_m describes the dependence of males on attained age a. In addition, $basq\_m$ relates to the quadratic age-dependence in males, associated with the term $\ln^2(a/50) \times \Theta(a-50)$. According to equation (S2) this expression is equal to $\ln^2(a/50)$ for attained ages larger or equal 50 years, otherwise it is zero. The remaining parameters are related to the linear and quadratic dependence from birth date b: bb_m and bb_f, for example, are the free parameters related to the linear dependence of male and female patients from birth year, respectively.

Because a limited amount of smoking information is available for only approximately 20% of the cohort, smoking was not included in the baseline model, in accordance with

Zablotska et al. (2014). The baseline model in equation (S4) contains the same explanatory variables as the stratified baseline model applied by Zablotska et al. (2014).

Mathematical functions used for the 11 parametric dose-response models from Figure 1

The general form of an ERR model is $h = h_0 \times (1 + ERR(D, Z))$, where h is the total hazard function, h_0 is the baseline model and $ERR(D, Z)$ describes the change of the hazard function with dose D allowing for dose-modification by association-modifying factor(s) Z. It is $ERR(D, Z) = err(D) \times \varepsilon(Z)$. Here, $err(D)$ describes the shape of the dose-response function, $\varepsilon(Z)$ contains the dose-effect modifiers. For h_0 the model in equation (S4) was applied.

For $err(D)$ the following dose-response models were used.

$$err(D) = \beta_1 \times D \qquad\qquad\qquad\qquad\qquad\qquad\qquad \text{LNT model}$$

$$err(D) = \beta_1 \times D^2 \qquad\qquad\qquad\qquad\qquad\qquad\qquad \text{Quadratic model}$$

$$err(D) = \beta_1 \times D + \beta_2 \times D^2 \qquad\qquad\qquad\qquad\qquad \text{Linear-quadratic model}$$

$$err(D) = \beta_1 \times D \times \exp(\beta_2 D) \qquad\qquad\qquad\qquad\quad \text{Linear-exponential model}$$

$$err(D) = \begin{cases} 0 & \text{for } D < D_{th} \\ \beta_1 \times (D - D_{th}) & \text{for } D \geq D_{th} \end{cases} \qquad\qquad \text{Linear threshold model}$$

$$err(D) = 0.5 \times scale \times [\tanh(s\,(D - D_{th})) - \tanh(-s\,D_{th})] \qquad \text{Smooth step model}$$

$$err(D) = \lambda_0 \left(1 - \frac{1}{1 + \left(\dfrac{D}{D_{th}}\right)^{\lambda_1}} \right) \qquad\qquad\qquad\qquad \text{Sigmoid model}$$

$$err(D) = \lambda_0 - \frac{\lambda_0 + \lambda_2 D}{1 + \left(\dfrac{D}{D_{th}}\right)^{\lambda_1}} \qquad\qquad\qquad\qquad \text{Hormesis model}$$

$$err(D) = \begin{cases} \beta_1 \times D & \text{for } D < D_{th} \\ \beta_1 \times D_{th} + \beta_2 \times (D - D_{th}) & \text{for } D \geq D_{th} \end{cases} \qquad \text{Two-line spline model}$$

$$err(D) = \beta_1 \times \exp\{-\beta_2 \exp[-\beta_3 \times (D - D_{th})]\} - \beta_1 \times \exp\{-\beta_2 \exp[-\beta_3 \times (-D_{th})]\} \quad \text{Gompertz model}$$

$$err(D) = \begin{cases} 0 & \text{for } D < 0.000001\,\text{Gy} \\ \beta_1 & \text{for } 0.000001 \leq D < 1\,\text{Gy} \\ \beta_2 & \text{for } 1\,\text{Gy} \leq D < 2\,\text{Gy} \\ \beta_3 & \text{for } 2\,\text{Gy} \leq D < 6\,\text{Gy} \\ \beta_4 & \text{for } D \geq 6\,\text{Gy} \end{cases} \qquad \text{Categorical model}$$

The hormesis model was introduced by Brain and Cousens (1989). Some adaptations to the model by Brain and Cousens (1989) were made by Cedergreen et al. (2005) and Simonetto et al. (2014) to yield the specific mathematical form applied in the present study.

Calculation of AIC-weights

For a set of n non-nested models, the AIC-weight, p_m, was calculated for model m according to the following equation (Burnham and Anderson 2002, Claeskens and Hjort 2008):

$$p_m = \frac{\exp\left(-\Delta \text{AIC}_m / 2\right)}{\sum_{j=1}^{n} \exp\left(-\Delta \text{AIC}_j / 2\right)} \quad \text{(S5)}$$

Here, $\Delta\text{AIC}_m = \text{AIC}_m - \text{AIC}_0$, where AIC_m is the AIC-value for model m and AIC_0 is the smallest AIC-value of all n models. The resulting weights, multiplied by a factor of 10^4, give the number of samples for risk estimates to be generated by uncertainty distribution simulations.

In the sparse model approach, nested dose-response models with inferior final deviances were eliminated by applying the LRT at a 95% confidence level (details related to this selection process are provided on pages 14-15 of the Online Resource). Subsequently, the criterion for inclusion of a model into the set of final non-nested models, which was used for multi-model inference (MMI), is whether $p_1 > 0.05$ when comparing with the best model, i.e. the one with $\Delta\text{AIC} = 0$ (6, 7). In that case equation (S5) reduces to $p_m = \exp(-\Delta\text{AIC}_m/2)/[\exp(-\Delta\text{AIC}_m/2) + 1]$ with $m = 1$. With this equation it is easy to show that for $\Delta\text{AIC}_1 < 5.9$ one obtains $p_1 > 0.05$. Applying this formula to the four final non-nested models for IHD mortality (Table 3, main text), one finds for the ERR-LNT, ERR-Q and ERR-two-line spline models $p_1 = 0.2503$, $p_1 = 0.4429$, and $p_1 = 0.4101$, respectively (refer to Table S3). Consequently, these three models together with the ERR-Gompertz model, which has the smallest AIC-value, survive the selection process. The AIC-weights provided in Table 3 (main text) for the models selected with the sparse model approach were calculated using equation (S5), i.e. they are normalized to 1 to be useful for MMI.

In the rich model approach, each model is compared with the best model (i.e. the one with $\Delta\text{AIC} = 0$), applying $p_m = \exp(-\Delta\text{AIC}_m/2)/[\exp(-\Delta\text{AIC}_m/2) + 1]$. Models with $p_1 > 0.05$ survive the selection process (Hoeting et al. 1999, Walsh 2007). The AIC-weights provided in Table 3 (main text) for the models selected with the rich model approach were calculated using equation (S5) because to be useful for MMI they need to sum up to 1.

For all dose-response models that were tested in the present study, the normalized and bilateral AIC-weights and all related details in the context of the sparse and rich model approaches are provided in Table S3.

Software

All analyses and model fits of the parametric baseline model (equation (S4)) combined with the dose-response models from Figure 1 and the MMI analyses (sparse and rich model approaches) were performed with MECAN, a C++-based software package (Kaiser 2010). It uses the maximum likelihood method and Poisson regression to estimate the values of the adjustable model parameters by fitting the model to the grouped CFCS data. Because maximizing the likelihood L is equivalent to minimizing the $-\ln(L)$, the latter problem, which is numerically better tractable, is solved in MECAN to find the best model solution. For grouped person-year data such as the grouped CFCS data, the likelihood corresponding to a Poisson model is used: $-\ln(L) = \sum_i \left[\Lambda_i - n_i + n_i \ln\left(n_i / \Lambda_i \right) \right]$ where n_i is the observed number

of cases (i.e. the number of fatalities from IHD) in group i and Λ_i is the calculated (expected) number of cases in group i. The deviance is defined as $dev := -2 \times \ln(\text{Max}L)$. Here, $\text{Max}L$ denotes the maximized likelihood. For the minimization of the deviance, MECAN applies the MINUIT package for function minimization (Moneta and James 2010).

ERR and *EAR* estimates can be calculated directly from h and h_0:

$$ERR = (h/h_0) - 1$$

$$EAR = h - h_0. \tag{S6}$$

Confidence intervals (CI) for the *ERR* and *EAR* estimates (both, for the final non-nested models that are included into Occam's group and for MMI) were simulated using multi-variate normal distributions for parameter uncertainties that obey the parameter correlation matrix (Kaiser and Walsh 2013). For a risk variable such as *ERR*, a probability density distribution of 10^4 realizations is generated, which is used to estimate 95% CI. Central risk estimates were calculated from the maximum likelihood estimates of the model parameters. The MECAN package and all model-related input and result files are available from the authors.
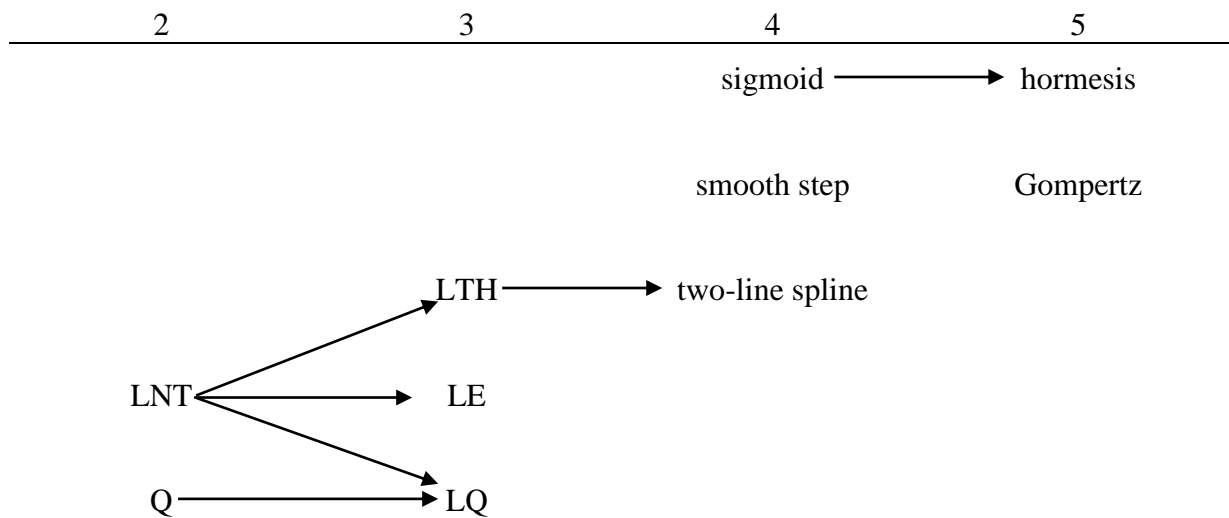
Figure S1 Number of model parameters in the dose-response models from Figure 1 and relation between the models (the categorical model is not shown because due to its higher number of model parameters and biologically implausible shapes it is not suited for MMI). Two models are nested if they are connected by an arrow. The smooth step model (modified hyperbolic tangent) and the Gompertz model are not nested with any of the other models. Here, parameter β_2 from equation (1) (main text) was counted as a model parameter for all the dose-response models because all of them contain it within the dose-effect modification.

Table S2 Model parameters, maximum likelihood estimates and Wald-type standard errors (in parenthesis) for the four final non-nested models that were identified for Occam's group and used for MMI (sparse model approach), Canadian Fluoroscopy Cohort Study, 1950-1987

#	Parameter[a]	ERR-LNT model[b]	ERR-Q model[b]
1	c_m	3.485 (0.144)	3.482 (0.144)
2	c_f	1.528 (0.208)	1.521 (0.208)
3	$prov\_m$	−0.2144 (0.0572)	−0.2138 (0.0571)
4	$prov\_f$	−0.1207 (0.0975)	−0.1182 (0.0975)
5	$cdur\_m$	−0.00662547[c]	−0.0111411[c]
5	$cdur\_f$	−0.00662547[c]	−0.0111411[c]
6	$diag\_m$	0.0224 (0.119)	0.0247 (0.119)
7	$diag\_f$	0.471 (0.147)	0.476 (0.147)
8	$nostg\_m$	0.0951 (0.119)	0.0949 (0.119)
9	$nostg\_f$	0.542 (0.140)	0.543 (0.140)
	$stg1\_m$	0	0
	$stg1\_f$	0	0
10	$stg2\_m$	0.0217 (0.0444)	0.0284 (0.0443)
11	$stg2\_f$	0.1256 (0.0696)	0.1331 (0.0695)
12	$stg3\_m$	0.0867 (0.0475)	0.0958 (0.0472)
13	$stg3\_f$	0.2937 (0.0742)	0.3028 (0.0740)
14	ba_m	5.885 (0.197)	5.879 (0.197)
15	ba_f	6.49457 (0.402)	6.492 (0.402)
16	$basq\_m$	−4.374 (0.398)	−4.372 (0.398)
17	$basq\_f$	−1.669 (0.687)	−1.673 (0.687)
18	bb_m (yr^{-1})	−0.1160 (0.0180)	−0.1138 (0.0180)
19	bb_f (yr^{-1})	−0.2716 (0.0282)	−0.2689 (0.0281)
20	$bbsq\_m$ (yr^{-2})	0.03931 (0.00821)	0.03884 (0.00821)
21	$bbsq\_f$ (yr^{-2})	0.0317 (0.0129)	0.0312 (0.0129)
22		$\beta_1 = 0.1823$ Gy^{-1} (0.0692)	$\beta_1 = 0.1420$ Gy^{-2} (0.0474)
23		$\beta_2 = -12.01$ yr Gy^{-1} (3.39)	$\beta_2 = -14.57$ yr Gy^{-1} (3.86)
	dev	13247.75	13246.01

#	Parameter[a]	ERR-two-line spline model[d]	ERR-Gompertz model[e,f,g]
1	*c_m*	3.449 (0.145)	3.479 (0.145)
2	*c_f*	1.493 (0.208)	1.507 (0.208)
3	*prov_m*	−0.2165 (0.0572)	−0.2180 (0.0572)
4	*prov_f*	−0.1192 (0.0976)	−0.1127 (0.0975)
5	*cdur_m*	−0.0409877[c]	−0.0208749[c]
5	*cdur_f*	−0.0409877[c]	−0.0208749[c]
6	*diag_m*	0.029 (0.120)	0.0232 (0.119)
7	*diag_f*	0.476 (0.147)	0.482 (0.147)
8	*nostg_m*	0.097 (0.119)	0.0930 (0.119)
9	*nostg_f*	0.541 (0.140)	0.544 (0.140)
	stg1_m	0	0
	stg1_f	0	0
10	*stg2_m*	0.0290 (0.0446)	0.0270 (0.0447)
11	*stg2_f*	0.1306 (0.0697)	0.1440 (0.0695)
12	*stg3_m*	0.0922 (0.0478)	0.0903 (0.0484)
13	*stg3_f*	0.2956 (0.0744)	0.3227 (0.0739)
14	*ba_m*	5.882 (0.198)	5.871 (0.198)
15	*ba_f*	6.489 (0.402)	6.499 (0.402)
16	*basq_m*	−4.371 (0.399)	−4.357 (0.399)
17	*basq_f*	−1.661 (0.687)	−1.695 (0.687)
18	*bb_m* (yr^{-1})	−0.1132 (0.0182)	−0.1152 (0.0182)
19	*bb_f* (yr^{-1})	−0.2693 (0.0282)	−0.2654 (0.0281)
20	*bbsq_m* (yr^{-2})	0.03934 (0.00822)	0.03914 (0.00824)
21	*bbsq_f* (yr^{-2})	0.0319 (0.0129)	0.0305 (0.0129)
22		$\beta_1 = 0.3571$ Gy^{-1} (0.0922)	$\beta_1 = 6.48$ (9.82)
23		$\beta_2 = 2.006$ Gy^{-1} (0.755)	$\beta_2 = 7.28$ (2.11)
24		$D_{th} = 1.7246$ Gy (0.0649)	$\beta_3 = 0.684$ Gy^{-1} (3.49)
25		$\beta_3 = -9.32$ yr Gy^{-1} (1.85)	$\beta_4 = -10.60$ yr Gy^{-1} (2.86)
			$D_{th} = 0$
	dev	13242.28	13241.55

[a] Parameters 1 to 21 are the baseline parameters, parameters 22 to 25 are the radiation-associated parameters.

[b] For the ERR-LNT and ERR-Q models parameter β_2 is related to the adjustment for dose-fractionation modifications (see equation (1) in the main text).

[c] The parameters *cdur_m* and *cdur_f* have been included into the baseline model to reflect their use in the dose-effect modifier but were not found to be significant. Therefore, they were fixed at their maximum likelihood estimates to stabilize the model fit. Without this fixation of *cdur_m* and *cdur_f* the parameter β_1 would have turned out to be not significant: For example, in the fit of the ERR-LNT model with *cdur_m* as a free parameter and *cdur_f* linked to it it was found that $\beta_1 = 0.182$ Gy^{-1} (0.111) with $p = 0.10$. The situation of other baseline parameters that were found to be not significant either such as, for example, *diag_m* is different. Whether allowing parameter *diag_m* to be free during a model fit or fixing it to

its maximum likelihood estimate, did not change the maximum likelihood estimates of the other free parameters (results not shown).

[d] For the ERR-two-line spline model the adjustment for dose-fractionation is associated with parameter β_3.

[e] For the ERR-Gompertz model the adjustment for dose-fractionation is associated with parameter β_4.

[f] It was found that for the fit of the Gompertz model the parameter D_{th} was not significantly different from zero. Therefore, D_{th} was fixed at zero. Consequently, this model has four radiation-associated model parameters (compare with Figure S1 where the five listed parameters still include D_{th}).

[g] It is noted that for the error calculations related to Figures 2 to 4 two of the dose-response parameters of the Gompertz model (β_2 and β_3) were fixed at their maximum likelihood estimates. Otherwise the 95% CI of the model-related risk predictions and in consequence the MMI-related 95% CI would turn out as too large.

Aspects of model selection according to the sparse model approach

Table 3 (main text) provides the main results of fitting the parametric dose-response models from Figure 1 as ERR models to the mortality data for IHD. Considering Figure S1 and applying the LRT four ERR models were identified according to the sparse model approach and were used for MMI. The selection process was performed as follows. The final deviance of the ERR-LNT model (13247.747) was compared with the final deviance of the parametric baseline model (dev = 13252.676). According to the LRT one would argue that adding model parameters β_1 and β_2 (see equation (1) in the main text) to the baseline model did not lead to a significant improvement of the fit at the 5% level because Δdev = 4.93 < 5.99. When comparing the final deviance of the ERR-Q model with the one of the parametric baseline model one finds Δdev = 6.66. The problematic of applying the LRT when comparing a baseline model with a dose-response model such as the LNT and Q-models that are multiplied with a dose-effect modifier (Liu and Shao 2003) is, however, known to the authors (in that case the LRT should not be applied because setting parameter $\beta_1 = 0$ also eliminates parameter β_2, which is contained in the dose-effect modifier). Both models (ERR-LNT and ERR-Q) were included into Occam's group for the following reasons: The ERR-LNT model because, when compared with the best model, it contains an AIC-weight larger than 0.05 (Walsh 2007): According to the formula given on page 8 of the Online Resource (p_m = exp(–ΔAIC$_m$/2)/[exp(–ΔAIC$_m$/2) + 1]) it is easy to see that p_1 = 0.25 (see Table S3). For the ERR-Q model one finds p_1 = 0.44 > 0.05. The ERR-LQ model is nested with the ERR-LNT and ERR-Q models (Figure S1). A comparison of the final deviances between ERR-LQ and ERR-LNT models yields Δdev = 2.36 < 3.84. Therefore, the additional parameter of the LQ model (β_2) is not statistically significant at the 5% significance level and consequently the ERR-LQ model was not included into the set of final non-nested models used for MMI. Analogous considerations hold for the ERR-LE model, which is nested with the ERR-LNT model: Δdev = 2.07 < 3.84. For the ERR-LTH model one compares with the ERR-LNT model to find Δdev = 0.93 < 3.84. Thereby, the ERR-LTH model was not included into the set of final non-nested models either. The smooth step model was implemented as a modified hyperbolic tangent function and is not nested with any of the other dose-response models (Figure S1). Therefore, its final deviance needs to be compared with the one of the baseline model: Δdev = 13252.676 – 13244.451 = 8.22. Because 8.22 < 9.49 this model was not included for MMI. The final deviance of the sigmoid model, not nested with any of the models that contain only two or three parameters (Figure S1), was compared with the final deviance of the baseline model to find Δdev = 6.74 < 9.49. Therefore, the sigmoid model did not survive the selection process as its four parameters were not significant. Although the hormesis model is nested with the sigmoid model, its final deviance needs to be compared with the final deviance of the baseline model because the sigmoid model was not significant. One obtains Δdev = 9.83 < 11.07. That eliminated the hormesis model. The two-line spline model is nested with the LTH model (Figure S1). The latter was, however, not significant. Consequently, comparison needs to be made with the baseline model and one finds Δdev = 10.39 > 9.49 (the bilateral weight of the two-line spline model turned out to be p_1 = 0.41 > 0.05; see Table S3). The problematic of applying the LRT in segmented regression (Feder 1975), as it is the case for the two-line spline model, is known to the authors. Instead of applying the LRT one would have to simulate the deviance-distributions of the two models (ERR-two-line spline and streamlined baseline models); if the two distributions do not overlap by more than 5%, then they are significantly different and consequently β_1, β_2 and D_{th} would be significant at the 95% level. Such in-depth analyses are, however, out of scope of the present study. Although

15

standard LRTs should not be applied for the two-line spline model, the latter was included into Occam's group based on the considerable reduction of the final deviance compared to the baseline model.

The Gompertz model is not nested with any of the applied models. Therefore, its final deviance needs to be compared with the final deviance of the baseline model. It was found that parameter D_{th} was not significant and was therefore set to zero. That reduced the number of parameters to four (compare with Figure S1). Because $\Delta \text{dev} = 11.12 > 9.49$ the ERR-Gompertz model was included into the set of final non-nested models.

The categorical model with its high number of parameters and biologically implausible shapes does not qualify for MMI. It was applied for a non-parametric characterization of the dose-response. It did, however, turn out that the risk prediction for the highest dose category (≥ 6 Gy; $ERR = 10.3$) was accompanied with a very large 95% CI. Therefore, the risk predictions from the categorical model are not shown in Figures 2 to 4 (instead, they are provided in the legend of Figure 2).

Table S3 Results of fitting the dose-response models from Figure 1 as ERR models to the mortality data for IHD including the two different types of AIC-weights, Canadian Fluoroscopy Cohort Study, 1950-1987 (Zablotska et al. 2014)

Sparse model approach								
Model	**dev**	**Δdev[a]**	N_{par}	**AIC[b]**	**ΔAIC[c]**	**Normalized AIC-weights[d]**	**Bilateral AIC-weights[e]**	**Rounded nsim[f]**
ERR-LNT	13247.75	6.19	23	13293.75	2.19	0.1183	0.2503	1183
ERR-Q	13246.01	4.46	23	13292.01	0.46	0.2815	0.4429	2815
ERR-two line spline, D_{th} = 1.72 Gy	13242.28	0.73	25	13292.28	0.73	0.2461	0.4101	2461
ERR-Gompertz, D_{th} = 0	13241.55	0	25	13291.55	0	0.3541		3541

Rich model approach[g]								
Model	**dev**	**Δdev**	N_{par}	**AIC**	**ΔAIC**	**Normalized AIC-weights**	**Bilateral AIC-weights**	**Rounded nsim**
ERR-LNT	13247.75	6.19	23	13293.75	2.19	0.0776	0.2503	776
ERR-Q	13246.01	4.46	23	13292.01	0.46	0.1847	0.4429	1847
ERR-LQ	13245.38	3.83	24	13293.38	1.83	0.0930	0.2859	930
ERR-LE	13245.68	4.13	24	13293.68	2.13	0.0802	0.2566	802
ERR-LTH, D_{th} = 0.58 Gy	13246.81	5.26	24	13294.81	3.26	0.0455	0.1639	455
ERR-smooth step, D_{th} = 4.47 Gy	13244.45	2.90	25	13294.45	2.90	0.0546	0.1902	546
ERR-sigmoid, D_{th} = 41.53 Gy	13245.94	4.39	25	13295.94	4.39	0.0259	0.1004	259
ERR-hormesis, D_{th} = 3.28 Gy	13242.84	1.29	26	13294.84	3.29	0.0449	0.1620	449
ERR-two-line spline, D_{th} = 1.72 Gy	13242.28	0.73	25	13292.28	0.73	0.1615	0.4101	1615
ERR-Gompertz, D_{th} = 0	13241.55	0	25	13291.55	0	0.2323		2323
ERR-categorical	13242.19	0.63	29	13300.19	8.63		0.0132	
Baseline	13252.68		21	13294.68				

[a] The difference in final deviance is denoted by Δdev with respect to the model with the smallest final deviance.

[b] AIC = dev + 2 × N_{par}, where N_{par} is the number of model parameters.

^{c} The difference in AIC-values with respect to the model with the smallest AIC-values is denoted by ΔAIC.

^{d} The normalized AIC-weights were calculated with equation (S5).

^{e} For the bilateral AIC-weights one model at a time is compared to the best model, i.e. the one with ΔAIC = 0, so that equation (S5) reduces to the following equation: $p_m = \exp(-\Delta AIC_m/2)/[\exp(-\Delta AIC_m/2) + 1]$ with $m = 1$ (refer to page 8 of the Online Resource). Except for the ERR-categorical model, all bilateral AIC weights of both the rich and the sparse model approaches exceed 0.05. Thus, all corresponding models are eligible for MMI.

^{f} The normalized AIC-weights, multiplied by a factor of 10^4, give the number of samples (nsim) for risk estimates to be generated by uncertainty distribution simulations.

^{g} For the error calculations within the rich model approach some of the dose-response parameters of 5 out of the 10 surviving models were fixed at their maximum likelihood estimates. Otherwise the 95% CI of the model-related risk predictions would turn out as too large.
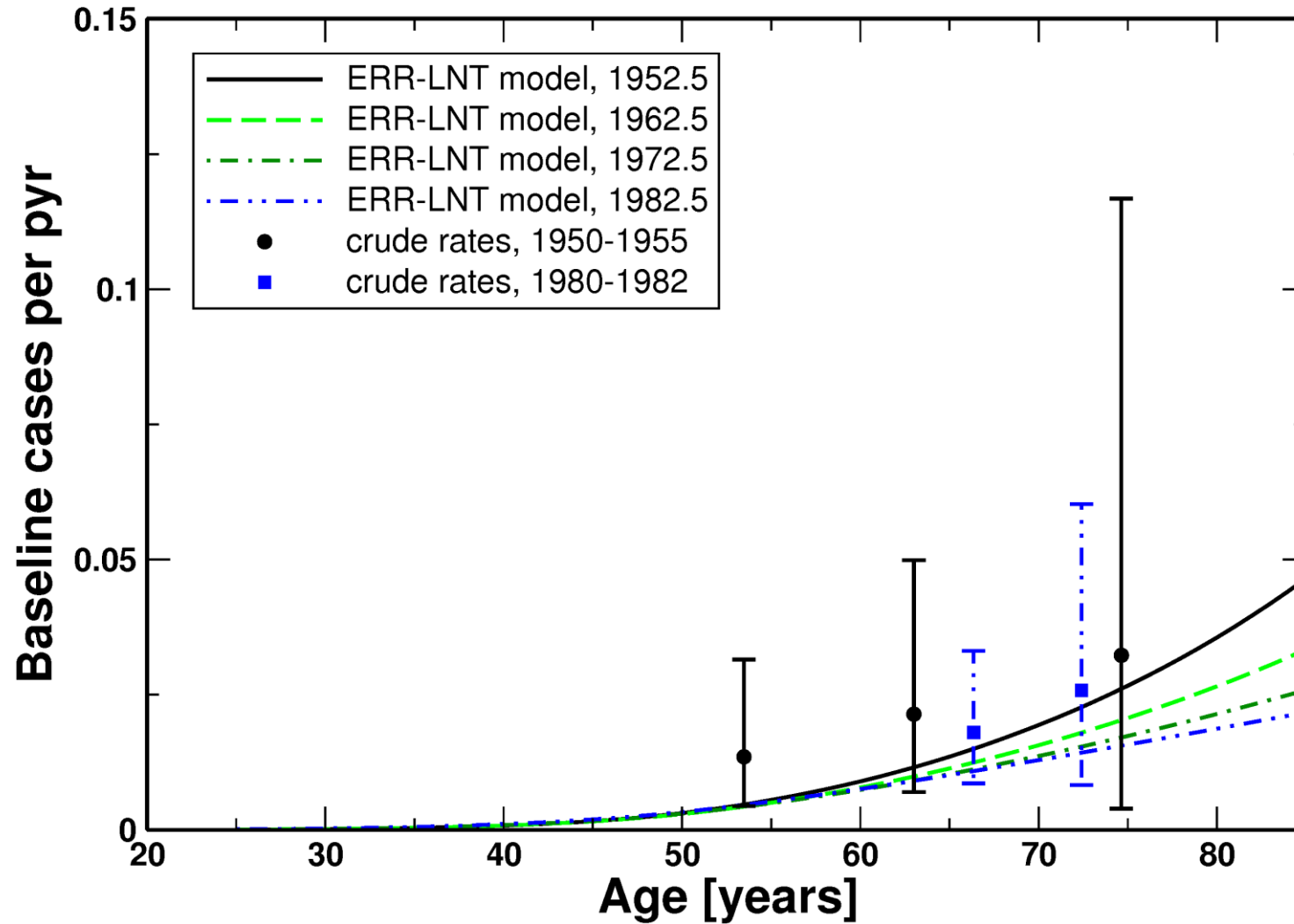
Figure S2 Baseline cases (i.e. baseline hazard h_0) per person-year as predicted by the ERR-LNT model plotted against attained age for calendar years 1952.5, 1962.5, 1972.5 and 1982.5. To produce the model predictions equation (S4) was evaluated with the maximum likelihood estimates

of the ERR-LNT model from Table S2. The model predictions are valid for non-smoking male tuberculosis patients admitted in the Canadian province of Nova Scotia, diagnosed with a minimal stage of nonpulmonary tuberculosis. The figure also shows crude rates (i.e. IHD cases divided by person-years), which were calculated for males admitted in the Canadian province of Nova Scotia with vanishing cumulative person-year-weighted lagged lung doses for specific age ranges and calendar year ranges (1950-1955, 1980-1985). For each of these age ranges the rates were plotted at the case-weighted mean ages. It is noted that for the crude rates it was not possible to select the same stratifications as for the model predictions because that would have resulted in low statistical power.

References

Brain P, Cousens R (1989) An equation to describe dose responses where there is stimulation of growth at low doses. Weed Res 29:93–96

Burnham KP, Anderson DR (2002) Model selection and multimodel inference, 2nd edn. Springer, New York

Cedergreen N, Ritz C, Streibig JC (2005) Improved empirical models describing hormesis. Environ Toxicol Chem 24:3166-3172

Claeskens G, Hjort NL (2008) Model selection and model averaging. Cambridge University Press, Cambridge

Feder PI (1975) The log likelihood ratio in segmented regression. The Annals of Statistics 3:84-97

Hoeting JA, Madigan D, Raftery AE, Volinsky CT (1999) Bayesian model averaging: a tutorial. Statist Sci 14:382–417

Kaiser JC (2010) MECAN. A software package to estimate health risks in radiation epidemiology with multi-model inference. User Manual. Version 0.2. Helmholtz Zentrum München, Neuherberg, Germany

Kaiser JC, Walsh L (2013) Independent analysis of the radiation risk for leukaemia in children and adults with mortality data (1950–2003) of Japanese A-bomb survivors. Radiat Environ Biophys 52:17–27

Liu BX, Shao Y (2003) Asymptotics for likelihood ratio tests under loss of identifiability. The Annals of Statistics 31, 807–832

Moneta L, James F (2012) Minuit2 minimization package. http://seal.web.cern.ch/seal/ snapshot/work-packages/mathlibs/minuit, April 2010. v. 5.27.02

Simonetto C, Azizova TV, Grigoryeva ES, Kaiser JC, Schöllnberger H, Eidemüller M (2014) Ischemic heart disease in workers at Mayak PA: latency of incidence risk after radiation exposure. PLOS One 9:e96309

Walsh L (2007) A short review of model selection techniques for radiation epidemiology. Radiat Environ Biophys 46:205–213